Volume 61
Number 91
25 November 2025
Pages 17703–17948

ChemComm

Chemical Communications

rsc.li/chemcomm

ISSN 1359-7345

ROYAL SOCIETY OF CHEMISTRY

HIGHLIGHT

Marzena Pander, Wojciech Bury *et al.*
When MOFs met SALI: solvent-assisted ligand incorporation in metal–organic frameworks for catalysis and beyond

ChemComm

HIGHLIGHT

View Article Online
View Journal | View Issue

Cite this: *Chem. Commun.*, 2025, **61**, 17715

When MOFs met SALI: solvent-assisted ligand incorporation in metal–organic frameworks for catalysis and beyond†

Marzena Pander, *[a] Emilian Stachura, [b] Magdalena Kozieł-Szymańska [b] and Wojciech Bury *[b]

Received 28th July 2025,
Accepted 25th September 2025

DOI: 10.1039/d5cc04299b

rsc.li/chemcomm

Solvent-assisted ligand incorporation (SALI) has emerged as a versatile and convenient post-synthetic modification (PSM) strategy for metal–organic frameworks (MOFs). By coordinating new ligands to unsaturated secondary building units (SBUs), SALI enables straightforward incorporation of a diverse range of organic ligands under mild conditions, avoiding the laborious synthesis often required in *de novo* approaches. Unlike many PSM methods relying on non-covalent or covalent modifications, SALI introduces functional ligands through direct dative bonds, making it broadly applicable in catalysis, gas separation, drug delivery, and beyond. This review provides a comprehensive overview of SALI advancements, highlighting its role in modifying MOFs and expanding their potential across various fields.

1. Introduction

The principles of reticular chemistry provide effective design strategies for the synthesis of materials tailored to specific applications.[1,2] Among these, metal–organic frameworks (MOFs), formed by connecting metal nodes with organic linkers, represent the largest subgroup, with over 100 000 reported structures.[3] MOFs have been widely explored for applications in sorption and separation processes,[4,5] heterogenous catalysis,[6,7] as drug delivery systems,[8] and sensors,[9,10] among others. Alongside the design of new MOFs, post-synthetic modification (PSM) strategies offer an unprecedented level of versatility for further functionalization and increase in structural complexity.[11,12] Importantly, PSM reactions can often be carried out under mild conditions, such as room temperature, enabling the incorporation of sensitive building units that would be challenging to introduce *via* conventional solvothermal synthesis. Another key advantage of PSM is its applicability to reported MOFs with well-established synthetic

[a] *Faculty of Chemistry, Jagiellonian University, Gronostajowa 2, 30-387 Kraków, Poland. E-mail: marzena.pander@uj.edu.pl*
[b] *Faculty of Chemistry, University of Wrocław, F. Joliot-Curie 14, 50-383 Wrocław, Poland. E-mail: wojciech.bury@uwr.edu.pl*

† This work is dedicated to the Faculty of Chemistry of the University of Wrocław on the occasion of its 30th anniversary.

Marzena Pander

Dr. Marzena Pander is currently working at the Faculty of Chemistry, Jagiellonian University in Kraków. In 2023, she completed her PhD in Chemistry at the University of Wrocław under the supervision of Professor Wojciech Bury, where she studied the post-synthetic modification of Zr-based MOFs. In the same year, she joined the research group of Professor Hoi Ri Moon at Ewha Womans University. Her current research focuses on the structural dynamics of responsive coordination polymers and their applications.

Emilian Stachura

Emilian Stachura received his MSc degree from University of Wrocław in 2020 under the supervision of Professor Wojciech Bury. He is currently a PhD student, working on desymmetrization of zirconium-based metal–organic cages and metal–organic frameworks.

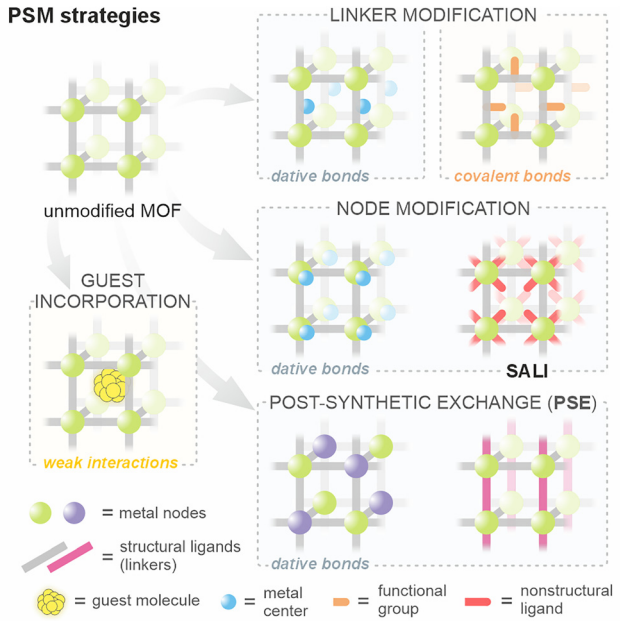

Fig. 1 Schematic overview and classification of post-synthetic modification (PSM) strategies in MOFs, categorized by the modified framework components and the type of interaction involved (covalent, dative, or non-covalent).

protocols, allowing for targeted functionalization without the need to develop new, time-consuming synthetic routes.[13]

Depending on structural features of the parent material and the desired properties of the daughter material, the introduction of new building blocks can be accomplished based on the dominant interactions between the MOF structure and the introduced molecules (Fig. 1). Accordingly, PSM strategies involve the formation of covalent or dative bonds, or the incorporation of guest molecules through weak interactions with the framework.[13] The strength of these interactions further determines the reversibility of the PSM step.

The potential lability of metal–ligand or metal-linker coordination bonds in MOF structures is well-recognized, particularly in their ability to undergo post-synthetic exchange of building blocks, where either metal centers within inorganic nodes or organic linkers can be replaced (Fig. 1).[14] Notably, in contrast to other PSM methods, the post-synthetic exchange (PSE) interferes with the structural integrity of the whole framework and can lead to either complete reconstruction of the material[15] or, when the exchange is incomplete, to a heterogeneous distribution of introduced moieties within the structure.[16,17] The selection of exchangeable subunits for PSE is dictated by the connectivity of the parent MOF. While other PSM methods offer broader versatility in this regard, the incorporation of new functional building blocks can reduce the porosity of the starting material.[18]

In general, PSM methods relying on dative bonds (Fig. 1) require the presence of either unsaturated metal centers capable of coordinating new ligands (or exchange them with labile ligands occupying these coordination sites) or organic linkers that can bind new metal cations.[19] The second strategy utilizes multiple coordination sites within selected organic linkers, which not only bind to the metal nodes of MOF but also can incorporate additional metal cations through donor atoms, as seen in linkers bearing porphyrin rings, bipyridyl moieties, catechols, and related chelators.[20] Alternatively, free metal coordination sites arise either from defects present in the synthesized material or as an inherited feature of the designed MOF structure.[21] The unoccupied coordination sites may remain vacant or be occupied by other labile ligands (*e.g.*, solvent or modulator molecules), which can be post-synthetically exchanged for new organic ligands or additional metal centers.[22] The coordination of new metal cations or organometallic complexes to the inorganic nodes of parent MOF introduces a secondary layer of metal centers, which often do not participate in linker coordination and hence serve a nonstructural role. This approach, leading to multimetallic

Magdalena Kozieł-Szymańska

Magdalena Kozieł-Szymańska received her MSc degree from University of Wrocław in 2023 under the supervision of Professor Wojciech Bury. She is currently a PhD student, working on free radical polymerization in metal–organic frameworks (FRaP-in-MOF).

Wojciech Bury

Dr. Wojciech Bury is an associate professor at the University of Wrocław, where in 2024 he became the leader of the Reticular Chemistry and Catalysis Group. He received his PhD degree in 2008 at Warsaw University of Technology, under the supervision of Prof. Janusz Lewiński. From 2011 to 2014, he completed a research internship at Northwestern University in the Hupp group, where he started his research adventure with MOFs. In 2016 he joined the Catalysis and Coordination Chemistry Group at the University of Wrocław, where he has been working on various aspects of reticular chemistry paying special attention to zirconium-based MOFs.

MOFs, is particularly important in the design and immobilization of efficient catalysts.[23]

In this highlight, we place a special focus on the PSM method involving the introduction of new nonstructural organic ligands through post-synthetic coordination to metal nodes, commonly referred to as the solvent-assisted ligand incorporation (SALI) technique. In the following chapters, we will explore reported SALI protocols that provide an unprecedented level of versatility for MOF functionalization, enabling a wide range of applications, including heterogeneous catalysis, sorption and separation, drug delivery, sensing, among others.

2. Solvent-assisted ligand incorporation (SALI) in MOFs

The term solvent-assisted ligand incorporation (SALI) was coined by Deria *et al*. in 2013 to describe an acid–base reaction between hydroxyl groups coordinated to the Zr_6-nodes of MOF and the carboxylate group of the external ligand (Fig. 2(b)).[24] As a result, the carboxylate ligand is coordinated to the metal centers. More broadly, SALI can be referred to the post-synthetic coordination of soluble organic ligands to the metal nodes of parent MOF through ligand exchange with more labile species (*e.g.*, solvent or modulator molecules, Fig. 2(a)). In early reports, post-synthetic coordination of nonstructural ligands to Zr-nodes was often described in terms of ligand installation,[25] ligand exchange,[26] defect engineering,[27] or post-synthetic modulator exchange,[28–30] particularly in connection with the removal of formates (originating from DMF decomposition) or other modulators coordinated to the metal nodes. Importantly, the incorporated ligands typically do not participate in the structural connectivity of the MOF and, for this reason, are commonly referred to as nonstructural ligands.

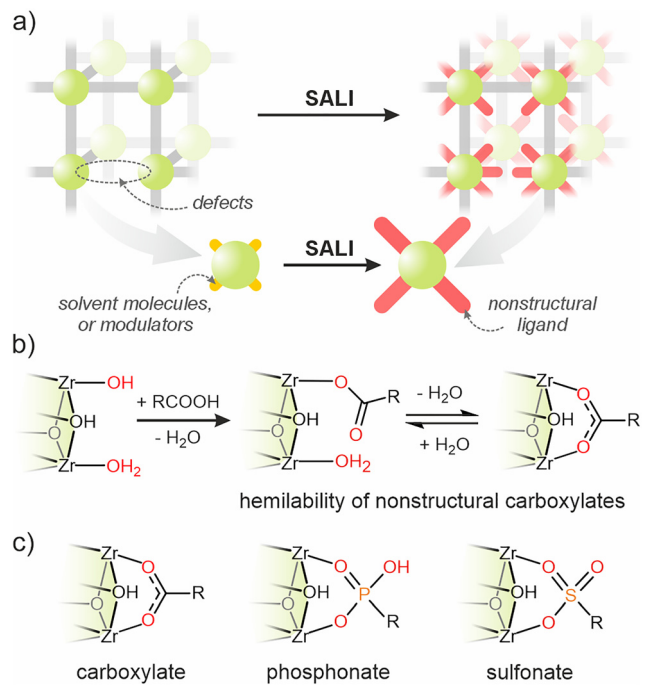

Fig. 2 (a) Scheme of SALI modification of metal nodes in MOFs. (b) Exemplified SALI reaction on Zr-node showcasing the hemilabile behavior of carboxylate nonstructural ligands. (c) Three types of ligands that were coordinated to Zr-nodes.

The development of the SALI approach and its rapid expansion toward other MOFs was prompted by the synthesis of Zr-based MOFs featuring Zr_6-nodes with lower connectivity.[31] The prototypical cuboctahedral Zr_6-nodes in these MOFs can coordinate up to 12 carboxylates, as exemplified by UiO-66, which features 12-connected Zr_6-nodes linked by terephthalate dianions.[32] In cases where the nodes are less than 12-connected, the unoccupied coordination sites can host reactive and exchangeable OH/H_2O pairs or small molecules such as solvents or modulators. Reduced node connectivity of Zr-MOFs[33] is often a consequence of linker geometry and synthetic conditions, which can yield Zr_6-nodes as low as 3- or 4-connected, as observed in Zr-MCMOF[34] and NU-1400,[35] respectively. Zr-based MOFs that have already become established platforms for SALI include NU-1000,[36,37] PCN-222,[38] MOF-808,[39] as well as defective 12-connected UiO-66,[32] NU-901,[40] and Zr-fum.[41]

The SALI protocol offers wide scope of the introduced molecules, with the only essential requirement being the presence of a structural motif capable of coordinating to the metal nodes.[42] As a result, a broad range of nonstructural ligands has already been implemented using SALI, including for example several chromophores for sensing and light-harvesting applications (Fig. 5(b) and 8(b)), biologically active molecules for drug delivery systems (Fig. 9(b)), and various chelating or hydrophobic ligands to modulate sorption and separation properties (Fig. 4(b) and 7(b)), among others. Notably, SALI can be performed under mild reaction conditions, enabling the successful coordination of temperature-sensitive molecules, such as the radical polymerization initiators (Fig. 10(b)),[43] molecular switches[44] or drug molecules in biocompatible solvents like water.[45] Moreover, a variety of organic molecules has been successfully introduced into MOFs for applications in heterogeneous catalysis. In these cases, the new ligands can enable or enhance the catalytic activity of SALI-modified MOF by supporting additional metal centers, introducing chirality, providing co-catalytic functionality, or tuning the node environment to improve substrate affinity. A more detailed discussion of SALI-modified MOFs, with emphasis on specific applications, will be provided in the following chapter.

Although the majority of ligands introduced *via* SALI are carboxylate-based, notable examples featuring other coordinating groups have been reported. These include, for example, phosphonates[46,47] and sulfonates,[48] which binding modes to Zr_6-nodes are presented in Fig. 2(c). It is worth noting that the compatibility between the pore dimensions of the functionalized MOF and the size of the introduced ligand also plays an important role in the SALI process. When a ligand is too large to access the internal pores, functionalization may be limited to the external surface of the crystallites.[49] In contrast, appropriate molecular sizing can enable modification of both the surface and interior of the framework. SALI-based surface

grafting thus offers a strategy for targeted functionalization while preserving internal porosity and maintaining pore accessibility for guest molecules.[50] Moreover, due to its thermodynamically controlled acid–base mechanism, SALI can enable a homogeneous distribution of functional groups throughout the crystal, even at low loading conditions,[51] provided the interior is accessible through diffusion.

The pK_a of modulators plays a crucial role in the crystalline phase formation during MOF synthesis.[52] Notably, this property is also relevant to the SALI protocol, where it has been observed that the exchange of nonstructural ligands occurs more readily when the pK_a of the introduced ligand is lower than that of the modulator already coordinated to the metal nodes.[42,53] Indeed, the post-synthetic exchange of modulators (monocarboxylates) coordinated to inorganic nodes can be readily utilized to functionalize selected materials.[28,54]

Additionally, as mentioned earlier, monodentate nonstructural ligands exhibit different lability compared to multidentate linkers that construct the MOF framework.[55,56] For example, in the case of monocarboxylic acids, coordination modes may involve one or both oxygen atoms interacting with the inorganic nodes (Fig. 2(b)). This feature plays a particularly important role in heterogenous catalysis, where the lability of nonstructural ligands can modulate access to active metal centers.[57,58] This is well illustrated by the SALI-based introduction of labile benzoates, which have been used as catalyst supports for Ni(II) cations in ethylene hydrogenation reaction.[59] The carboxylate shift of monocarboxylates coordinated to Zr_6-nodes depends also on the nature of the ligand. Rayder *et al.* demonstrated this by comparing acetic acid and trifluoroacetic acid (TFA) coordinated to the Zr_6-nodes of MOF-808, where the difference in ligand behavior significantly influenced the affinity of the modified material for CO_2 adsorption.[60]

Finally, to extend the complexity and usability of SALI-modified MOFs, it is worth noting that the introduced nonstructural ligands can undergo further transformations (secondary functionalization). These ligands may be further modified similarly to other PSM strategies (Fig. 1). Such tandem PSM approaches have been demonstrated in SALI-modified MOFs, including reactions such as alkylation of pyridine-based carboxylates,[61] click reactions with azide derivatives,[26] or further metalation of chelating ligands,[62] among others. This approach significantly expands the functionality of SALI-derived materials, enabling their tailoring for specific properties and target applications.

3. SALI-modified MOFs in heterogeneous catalysis

Post-synthetic modification of MOFs *via* SALI has enabled the development of advanced heterogeneous catalysts through the precise incorporation of nonstructural ligands at the metal nodes.[63] We identify four distinctive functions that these ligands can introduce within SALI-functionalized MOFs, which will be discussed in the following subchapters. These include the introduction of Brønsted or Lewis acid/base sites, immobilization of catalytically active metal centers, facilitation of light-induced charge or energy transfer for photocatalysis, and incorporation of chiral motifs to promote enantioselective transformations. These strategies exemplify the versatility of the SALI platform in designing multifunctional materials tailored to specific catalytic applications.

Pioneering studies on PSM of metal nodes date back to the early 2000s, coinciding with the emergence of MOF chemistry. It has been demonstrated that coordinatively unsaturated Cr(III) sites in MIL-101 could accommodate N-donor ligands, such as amines,[64–67] pyridines,[68] imidazoles,[69] and ionic liquids,[70–72] leading to improved catalytic performance. Similarly, the open metal sites of CuBTC (HKUST-1) were functionalized with N-donor ligands to create multifunctional catalysts, including pyridine derivatives,[73,74] Schiff bases,[75] and ionic liquids.[76]

3.1. Heterogenous acid–base catalysts

Acid–base catalysis represents a broad class of chemical transformations in which the reaction is accelerated by the presence of an acid or a base. The catalytic steps can occur *via* Brønsted- or Lewis-based pathway, where the donor–acceptor affinity towards protons or lone electron pairs, respectively, is the driving force of the catalytic cycle (Fig. 3(a)). Both Brønsted and Lewis acid/base sites can be incorporated in MOFs through the precise design of the framework or *via* post-synthetic strategies.[6] In this regard, the SALI method offers a versatile platform for introducing acidic or basic functionalities directly at the metal nodes, enabling their use in heterogeneous acid–base catalysis.

One of the pioneering studies on the synthesis of superacidic MOFs in SALI-like fashion was carried out by Jiang *et al.*, who prepared MOF-808-2.5SO_4 by treating parent MOF-808 with aqueous sulfuric acid (**L1**).[77] The measured Hammett acidity function (H_0) for the obtained material was ≤ -14.5, surpassing a conventional superacid threshold. The strong acidity was attributed to the presence of Zr-bound sulfate groups, and the resulting MOF was found to be catalytically active in several reactions including Friedel–Crafts acylation, esterification and isomerization.[77] Building on this approach, a Hf-based analogue of MOF-808 was functionalized in a similar manner with sulfuric acid (**L1**), exhibiting enhanced catalyticactivity in the solvent-free synthesis of benzoxazoles[79] and in the acetalization of benzaldehyde with methanol.[80]

Later, Trickett *et al*. investigated the origin of strong Brønsted acidity in sulfated MOF-808, identifying that a hydrated structure, consisting of adsorbed water and sulfate groups on Zr-nodes, generated the strongest acid sites.[78] A significant loss of acidity upon dehydration emphasized the critical role of coordinated water molecules in stabilizing the active acid sites. The hydrated and sulfonated MOF-808 showed excellent catalytic performance in the dimerization of isobutene, achieving 100% selectivity toward C_8 products (Fig. 3(c)). In contrast, the work by Yang *et al.* indicated a strong correlation between the stability of the conjugate base and proton affinity, suggesting that the local coordination environment is a key factor in determining the strength of the acid sites.[81] A similar approach was employed to functionalize NU-1000 with phosphoric acid (**L2**), enhancing its

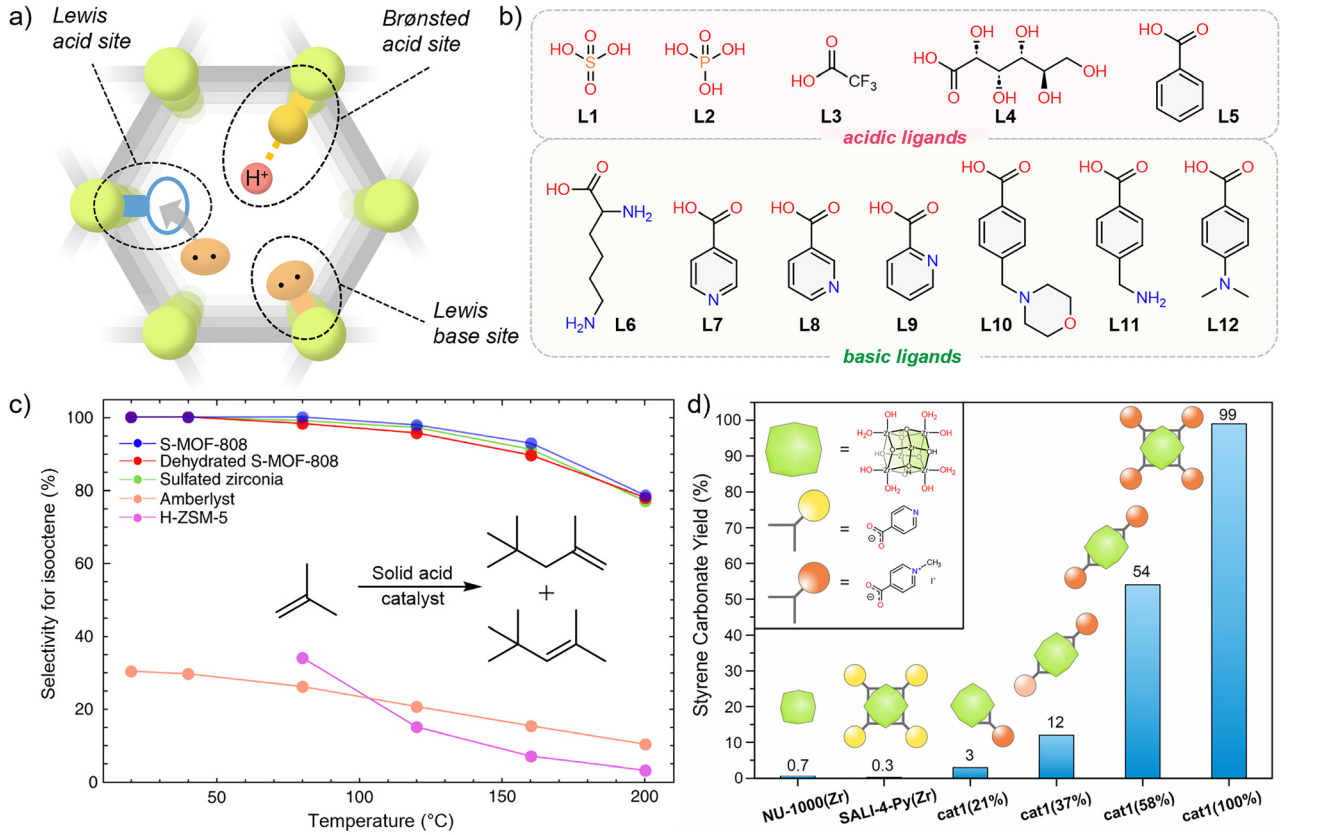

Fig. 3 (a) Scheme of possible SALI modifications of MOF with Brønsted acid, Lewis acid or base. (b) Examples of acidic and basic ligands introduced into MOF *via* SALI. (c) The selectivity for isooctane over other higher oligomers for Amberlyst, Z-ZSM-5, sulfated zirconia, sulfated MOF-808 (S-MOF-808) and dehydrated S-MOF-808.[78] Figure adapted form ref. 78 with permission. Copyright 2019 Springer Nature. (d) Influence of the amount of pyridinium moieties introduced into NU-1000 on the catalytic activity in the formation of styrene carbonate; cat1 = MeI-L7@NU-1000.[61] Figure adapted form ref. 61 with permission. Copyright 2021 American Chemical Society.

catalytic activity and promoting selective dehydration of glucose to afford a high yield of 5-hydroxymethylfurfural.[82]

Besides Brønsted acidity, SALI can also be used to tune the Lewis acid properties of MOFs (Fig. 3(a)). For example, Wang *et al.* functionalized MOF-545 with trifluoroacetic acid (TFA, **L3**) or benzoic acid (BA, **L5**), demonstrating that coordination of TFA to Zr_6-nodes enhanced the catalytic activity of the material in the ring-opening reaction of epoxides with methanol.[83] Moreover, the simultaneous presence of both, Lewis acid and base sites, can be beneficial in tandem, one-pot reactions. For instance, MOF-808, with Zr_6-nodes acting as Lewis acid sites, was functionalized with lysine (Lys, **L6**) as Lewis base, and tested in a cascade of Henry/Friedel–Crafts reactions between benzaldehyde, nitromethane, and indole, affording 3-(1-phenyl-2-nitroethyl)indole in high yield.[84]

Hydrolysis of organophosphorus compounds (OPCs), a major class of chemical warfare agents, is another example that benefits from the cooperative presence of Lewis acid and base functionalities. Typically, detoxification of OPCs using Zr-based MOFs requires alkaline conditions to regenerate the catalytically active Zr-sites and avoid catalyst poisoning.[85] To overcome this limitation, Garibay *et al.* modified NU-901 and MOF-808 with various amine-containing benzoic acids (**L7**, **L10–L12**) featuring different p*K*a values. The resulting SALI-modified MOFs enabled efficient hydrolysis of dimethyl 4-nitrophenyl phosphate (DMNP) and ethyl *N*-2-diisopropylaminoethyl methylphosphonothiolate (VX) under bufferless aqueous conditions within minutes.[86] In a follow-up study, the same group compared the catalytic performance of Hf- and Zr-based MOF-808 derivatives modified *via* SALI with 4-(morpholinomethyl)benzoic acid (**L10**), 4-(aminomethyl)benzoic acid (**L11**) and 4-(*N*′-hydroxycarbamimidoyl)benzoic acid.[87] While all of the modified MOFs showed improved catalytic activity, Hf-based analogues showed higher efficiency in DMNP hydrolysis.

A similar cooperative effect is observed in the cycloaddition of CO_2 to epoxides, a catalytic reaction that typically requires the presence of both Lewis acid and base sites, and thus often relies on the addition of external cocatalysts. The SALI technique enables direct incorporation of Lewis base sites (cocatalyst) into MOF structure, as demonstrated by a two-step post-synthetic modification of NU-1000. In this approach, pyridine-carboxylic acids (**L7–L9**) were first coordinated to the Zr-nodes, followed by *N*-alkylation with various alkyl halides.[61] The resulting series of bifunctional catalysts were tested in solvent-free cycloaddition of CO_2 to a range of epoxides under mild

conditions, achieving up to 99% yield of styrene carbonate at room temperature (Fig. 3(d)). In a related example, defective UiO-66 was functionalized with D-gluconic acid (**L4**), which improved both CO_2 uptake and catalytic activity in CO_2 conversion with epichlorohydrin.[88]

3.2. Mono- and multimetallic catalysts

MOFs can serve as effective supports for metal cations (M^{n+}) or metal nanoparticles (NPs) (Fig. 4(a)). Metal cations can be precisely anchored to the binding groups of linkers or nonstructural ligands introduced within the framework.[19] Similarly, MOFs can stabilize metal NPs by improving their uniform dispersion and preventing aggregation.[89] The introduction of additional metal centers can enable or enhance catalytic activity and facilitate tandem transformations within a single catalyst.

The SALI technique provides a convenient strategy to introduce metalated ligands (Fig. 4(b)) directly into the MOF structure, allowing the immobilization of new catalytic sites. For example, Li *et al.* deposited NU-1000 thin film on glassy carbon electrode and subsequently functionalized it with a rhodium complex (**L22**), enabling its application in electrochemical NADH regeneration.[91] Optimization of the Rh-catalyst loading in this material led to high electrocatalytic activity, achieving high faradaic efficiency of 97% and turnover frequency (TOF) of approximately 1400 h^{-1} for NADH regeneration. A related system, in which surface deposited NU-1000 modified with an analogous Rh complex was combined with a gas diffusion electrode that provided a clean proton source for NADH regeneration.[92] Both of these setups enabled efficient electrochemical regeneration of NADH and supported enzymatic

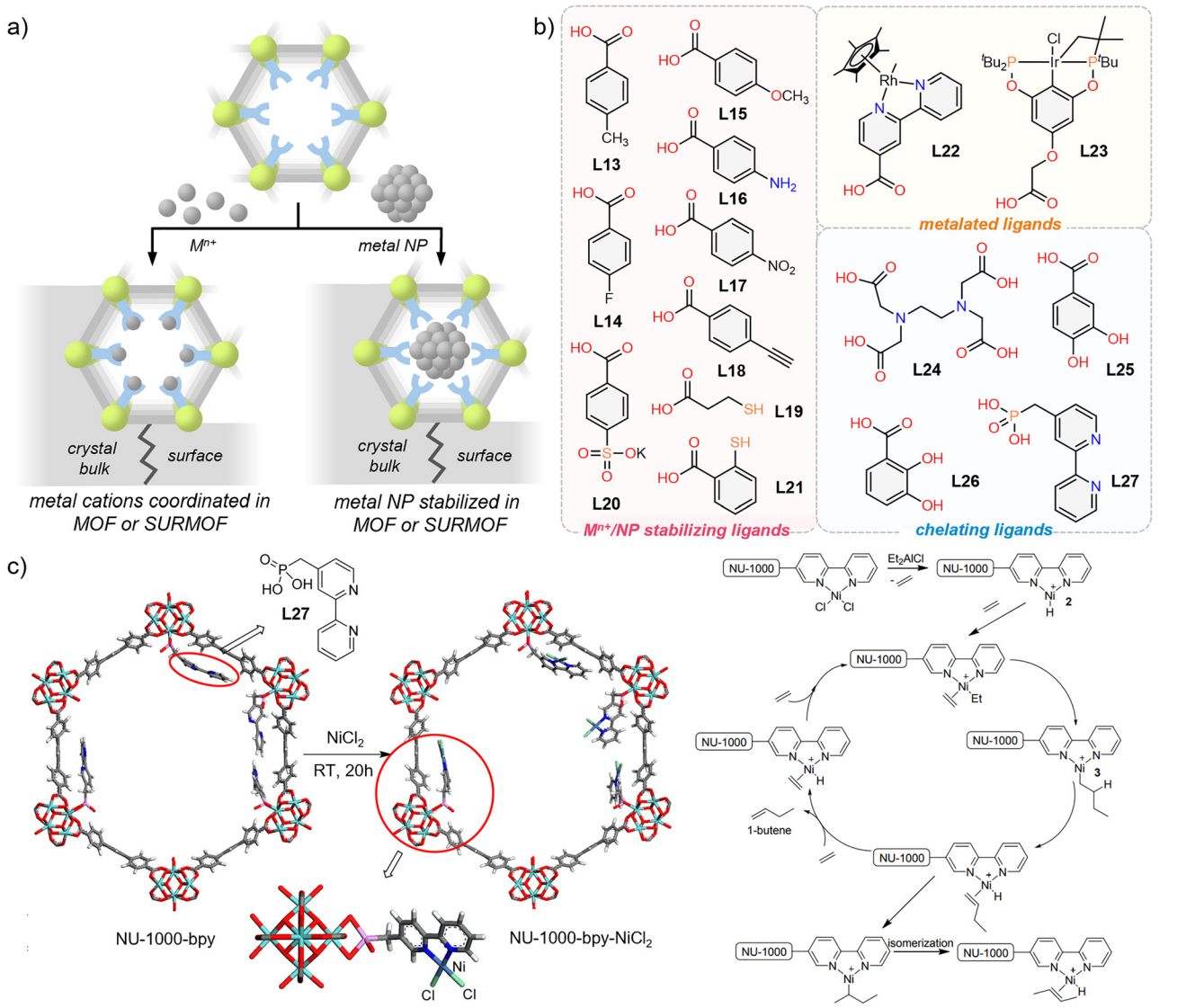

Fig. 4 (a) Scheme of functionalization of SALI-modified MOF as support for metal ions or metal nanoparticles. (b) Representative examples of metalated, chelating and stabilizing nonstructural ligands. (c) Scheme of two-step modification of NU-1000 with **L27** and metalation with Ni(II) centers (left) and catalytic cycle for dimerization ethylene with modified NU-1000-bpy-$NiCl_2$.[90] Figure adapted form ref. 90 with permission. Copyright 2015 American Chemical Society.

L-lactate production using L-lactate dehydrogenase as a model reaction. In another example, an iridium pincer complex (**L23**) was incorporated into NU-1000 *via* SALI, where spectroscopic studies confirmed the formation of active iridium dihydride species.[93] The resulting material catalyzed the hydrogenation of liquid alkenes (1-decene and styrene) with higher activity than its homogeneous analogue and operated as a heterogeneous catalyst under flow conditions. In another study, isonicotinic acid (**L7**) was incorporated at the Zr-nodes of NU-1000, providing binding sites for an iridium complex. The resulting material was used as heterogeneous catalyst for *p*-H_2 to *o*-H_2 isomerization. and produced anomalously large antiphase NMR signals for hyperpolarized *o*-H_2.[94]

Metal cations can be introduced after SALI by interacting with pre-installed chelating ligands (Fig. 4(b)). For instance, Madrahimov *et al.* modified NU-1000 in a two-step process by first incorporating 5-methylphosphonate-2,2′-bipyridine (**L27**) *via* SALI, followed by metalation with $NiCl_2$ (Fig. 4(c)).[90] Subsequent activation with Et_2AlCl afforded a single-site catalyst for ethylene dimerization, exhibiting an order of magnitude higher activity than its homogeneous analogue, along with good recyclability under both batch and flow conditions.

Similarly, ethylenediaminetetraacetic acid (EDTA, **L24**) was introduced into MOF-808 *via* SALI to enable post-synthetic metal cations incorporation. The resulting material exhibited high catalytic efficiency in Suzuki coupling reactions, with conversion and selectivity reaching 99%.[95] MOF-808 was also functionalized with catechol–benzoate ligands (2,3- and 3,4-dihydroxybenzoic acid, DHBA, **L25**, **L26**) and subsequently metalated with Cu(I) precursors.[96] The resulting materials catalyzed 1,3-dipolar cycloadditions between azides and alkynes with good yields and 1,4-regioselectivity, where Cu-2,3-DHBA-MOF-808 showed superior performance across a broad range of substrates.

Alternatively, Zr-nodes of NU-1000 were post-synthetically modified with a series of *para*-substituted benzoates (**L13–L17**), followed by the introduction of Ni(II) centers.[59] These materials were tested as catalysts for ethylene hydrogenation, and the catalytic activity could be tuned by altering the electronic and steric environment of the Ni sites by the nonstructural ligands. Importantly, observed variations in ligand binding modes (Fig. 2(b)) enabled tuning of the hydrogenation activity.

The SALI strategy has also enabled the construction of single-site heterogeneous catalysts by stabilizing introduced metal centers. One representative example was demonstrated by Rosado *et al.*, where the NU-1000 derivative bearing amino groups was functionalized with 3-mercaptopropionic acid (**L19**) and subsequently impregnated with Cu^{2+} ions. The obtained material was then thermally reduced under H_2 to obtain dispersed Cu^+/Cu^0 single-atom sites stabilized by the interaction with thiolate groups. The resulting catalyst was tested in CO_2RR processes where formic acid was identified as the main product.[97] Similarly, Otake *et al.* incorporated Pd(II) into phosphated or sulfated Hf-MOF-808.[98] Spectroscopic analyses and density functional theory (DFT) calculations confirmed that the acidic functionalities not only stabilize the active Pd(II) species but also suppress Pd(0) aggregation by stabilizing reaction intermediates. As a result, the modified MOFs exhibited improved catalytic activity in the oxidative Heck reaction of 2-phenylphenol with ethyl acrylate, compared to non-functionalized Hf-MOF-808.

Finally, SALI also provides an effective strategy to modify MOFs with stabilizing ligands that allow uniform dispersion of metal NPs. For example, Au NPs were prepared in the pore system of NU-1000 by a three-step process, where 4-carboxyphenylacetylene (**L18**) was used as a stabilizing ligand. The obtained NU-1000-Au-nano was tested as a catalyst for hydrogenation of 4-nitrophenol to 4-aminophenol.[99] Later, Muhamed *et al.* functionalized NU-1000 with 2-mercaptobenzoic acid (**L21**) to support the growth of gold[100] and silver[101] NPs. The resulting hybrid materials showed high efficiency in the hydrogen evolution reaction (HER) and strong cycling stability over 36 hours.[100] In the case of silver, the NPs formed through coordination of Ag(I) with thiol group of **L21** in NU-1000. The resulting composite contained ~95% Ag(0) and exhibited good activity in HER.[101] Similarly, NU-902 was first modified with 4-sulfobenzoic acid potassium salt (**L20**), followed by deposition of Ag NPs, to construct a highly efficient electrochemical nitrite sensor.[102] In the resulting material, both the porphyrin-based linkers and Ag NPs contributed to enhanced electrocatalytic nitrite oxidation. The thin film sensor, based on this composite, exhibited high selectivity against common ionic interferents, making it a promising sensor for nitrite detection.

3.3. Photocatalysts

MOF materials emerged as promising photocatalysts due to their ability to incorporate active sites for efficient light absorption and charge separation (Fig. 5(a)). Among various light-driven transformations, photocatalytic reduction of CO_2 is an important process for converting greenhouse gas into valuable products. Karmakar *et al.* investigated the photocatalytic reduction of CO_2 to CH_4 in water using functionalized MOF-808.[103] To enhance the photoactivity of this material, 1-pyrenebutyric acid (**L28**) was grafted to the Zr-nodes, followed by incorporation of methyl viologen to form donor–acceptor charge transfer (CT) supramolecular complex within the MOF pores. The resulting hybrid material exhibited red-shifted CT absorption at 540 nm and showed high selectivity towards CH_4 formation under the sunlight (Fig. 5(d)). The good efficiency and durability of the photocatalyst were attributed to the synergistic MOF-CT interaction and the protective effect of the MOF structure.

In a more recent example, Haimerl *et al* reported the incorporation of spiropyran (SP) derivative (**L29**) into NU-1000 *via* SALI.[104] Upon UV irradiation, closed-ring SP undergoes a reversible ring-opening to form its isomer, merocyanine (MC, Fig. 5(c)). To investigate the switch between energy transfer (EnT) and CT pathways, the resulting NU-1000-SP was probed in phosphinylation reaction between diphenylphosphine oxide and 1,1′-diphenyletylene. The study demonstrated that NU-1000-SP allowed modulation of products distribution by tuning the ET/CT pathways ratio, which is dependent on the used wavelength.

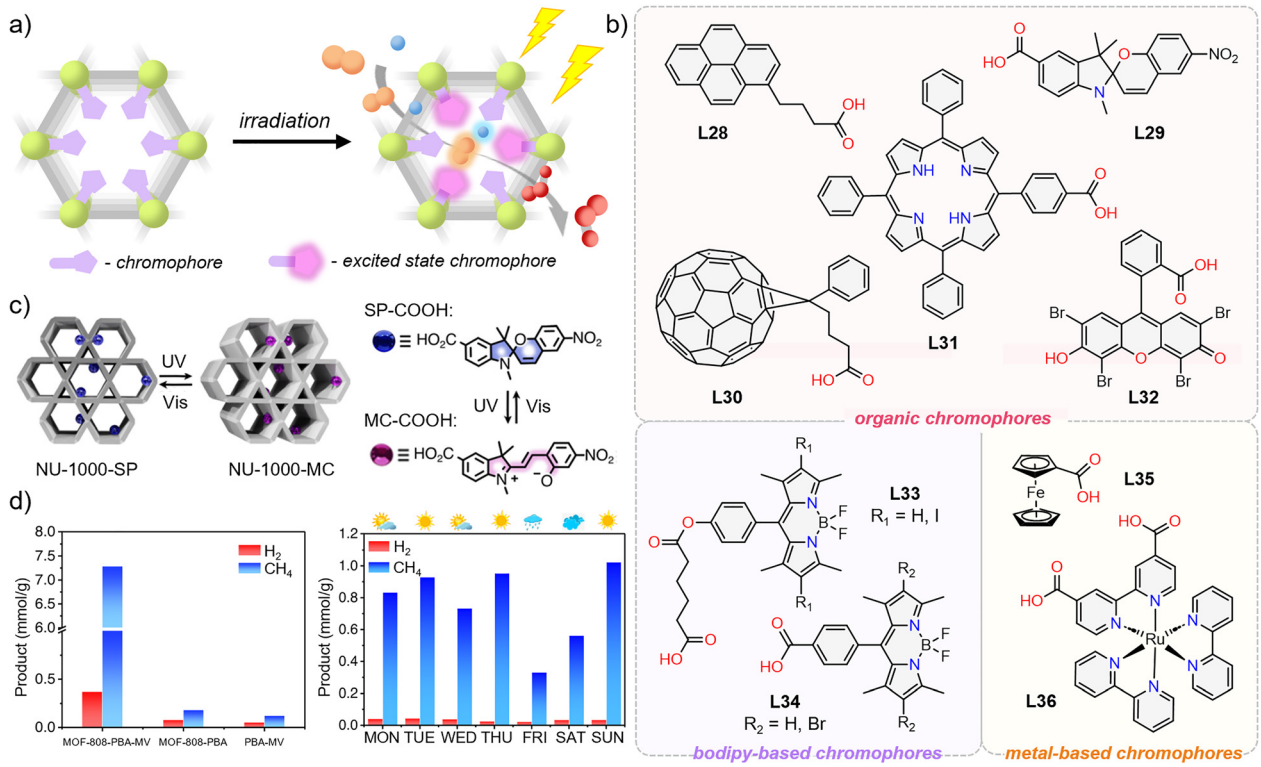

Fig. 5 (a) Scheme of excitation of introduced ligands *via* SALI for photocatalysis. (b) Representative examples of organic, metal-based and BODIPY-based chromophores used in SALI. (c) Scheme of reversible ring opening reaction of **L29** grafted into NU-1000 under UV irradiation.[104] Figure adapted form ref. 104 with permission. Copyright 2025 American Chemical Society. (d) Graphs displaying CH_4 over H_2 formation using MOF-808 modified with **L28** and methyl viologen.[103] Figure adapted form ref. 103 with permission. Copyright 2023 Springer Nature.

SALI modification has been also employed to develop photocatalysts capable of singlet oxygen generation for detoxification of chemical warfare agents. Howarth *et al*. reported the functionalization of NU-1000 and NU-1200 with phenyl-C_{61}-butyric acid (**L30**), a C_{60} derivative that efficiently generates singlet oxygen.[105] The resulting materials were tested as photosensitizers for the oxidation of sulfur mustard (HD) and its simulant, 2-chloroethyl ethyl sulfide (CEES). The oxidation of CEES was highly efficient, achieving over 90% conversion within minutes, while oxidation of HD was slower, reaching similar conversion in over 40 minutes. The same ligand (**L30**) was later incorporated into mixed-ligand MOFs containing chromophore linkers based on porphyrin and pyrene.[106] These systems exhibited sequential energy and charge transfer which was exploited in the photooxidation of sulfides to sulfoxides. In the presence of the prepared catalyst, thioanisole was converted to the corresponding sulfoxide within 6 h with 94% yield. Very recently, Jin *et al*. integrated porphyrin (**L31**) in a Zr-MOF based on naphthalene diimide (NDI), resulting in a donor–acceptor CT system, Zr-NDI-L31, which was highly efficient in photocatalytic oxidative hydroxylation of arylboronic acids and oxidative homocoupling of amines.[107]

Boron-dipyrromethene (BODIPY) dyes and especially their halogenated derivatives are well-known photosensitizers for singlet oxygen generation.[108] Incorporating the bromo-BODIPY ligand (**L34**) into NU-1000 significantly improved its singlet oxygen production, enabling oxidation of CEES to its less toxic sulfoxide derivative within nine minutes under green LED (450 nm) irradiation.[109] In a related study, the iodo-BODIPY derivative (**L33**) was introduced into NU-1000 using SALI.[110] The complementary spectral properties of the pyrene-based linker and BODIPY ligand enabled efficient EnT and facilitated photocatalytic generation of singlet oxygen, as demonstrated by the oxidation of 1,5-dihydroxynaphthalene to 5-hydroxy-1,4-naphthalenedione (Juglone) under visible light irradiation. In a distinct photocatalytic system, the organic dye eosin Y (**L32**) was incorporated into MOF-808 *via* SALI to improve its performance in oxidation of alcohols under visible light.[111] The resulting material enabled efficient activation of $C(sp^3)$–H bonds and molecular oxygen, promoting oxidation of alcohols with up to 99% selectivity for aldehydes over carboxylic acids.

The Ru(II) centers, known for their redox activity and efficient excited-state electron transfer properties, can serve as catalytic sites under visible light irradiation. Nagatomi *et al.* investigated the integration of Ru(II) with NU-1000 to enhance its photocatalytic activity in oxidative amine coupling.[112] The Zr-nodes of this material were functionalized with the photoactive tris(2,2′-bipyridine)ruthenium(II) complex, $[Ru(bpy)_3]^{2+}$ (**L36**). The resulting material enabled almost quantitative conversion of (4-methylphenyl)methylamine within 1 hour under blue LED irradiation, compared to 24 hours required by the homogeneous Ru(II) complex. Moreover, the redox-active ligand

L36 was also incorporated into the redox-inert NU-1008 to investigate its role in the CT process.[113]

Better understating of the CT mechanisms is of paramount importance for developing MOFs for electrocatalytic or energy storage applications.[114] In this context, ferrocene carboxylic acid (**L35**) is often selected as redox-active probe that has been introduced *via* SALI into various Zr-MOFs, including NU-1000,[115,116] PCN-222 and SIU-100,[51] or at defective Zr-nodes of UiO-66.[117] It was recently demonstrated that functionalization of defective UiO-66-NH_2-with **L35** enhances photocatalytic CO_2 reduction under visible light.[118] While the presence of ferrocene improves light absorption and facilitates ligand-to-metal CT, it also partially inhibits the Lewis acidity of Zr_6-nodes. By balancing these effects, the optimized MOF achieved efficient CO_2 to CO conversion.

3.4. Chiral catalysts

Chiral MOFs (CMOFs) have emerged as valuable asymmetric catalysts for the synthesis of enantiomerically pure compounds (Fig. 6(a)). Besides the often challenging *de novo* synthesis of CMOFs, PSM strategies offer a convenient tool for introducing chirality into achiral MOFs. A pioneering example of post-synthetic incorporation of chiral ligands into MOF was reported by Banerjee *et al.* in 2009, who modified MIL-101(Cr) with L-proline derivatives for use in asymmetric catalysis.[119] The resulting CMOFs showed good activity in asymmetric aldol condensation, reaching up to 90% conversion with ~70% enantiomeric excess (ee), surpassing the activity of the free chiral ligand. In a related study, N-functionalized L-proline derivatives were introduced into MIL-101(Cr) to catalyze the asymmetric reduction of ketimine with moderate conversion of 81% and 37% ee after 24 h at room temperature.[120]

Chiral nonstructural ligands can be incorporated through SALI[29,121,122] or used as modulators during MOF synthesis,[123–125] and typically include α-hydroxy acids and α-amino acids (Fig. 6(b)). For example, NU-1000 was modified with L-tartaric acid (**L37**) *via* SALI, followed by incorporation of a Mo(VI) complex.[126] The resulting material demonstrated excellent catalytic activity in asymmetric olefin epoxidation performance, reaching up to 100% selectivity and 85% ee.

Similarly, a series of CMOFs were obtained by grafting (*R*)-2-hydroxy-2-phenylacetic acid (**L38**), (*R*)-2-hydroxy-3-phenylpropionic acid (**L39**) and (*R*)-2-hydroxy-4-phenylbutanoic acid (**L40**) to Zr-nodes of PCN-222(Cu).[127] These catalysts afforded nearly quantitative yields in the asymmetric ring-opening reaction of cyclohexene oxide with aniline, with the best-performing derivative **L40** reaching 83% ee.

Sha *et al.* used SALI to introduce L- and D-histidine (**L43**, **L44**) into MOF-808, followed by Cu(II) coordination to mimic catechol oxidase active sites (Fig. 6(c)).[128] The modified material catalyzed the oxidation of various catechols to quinones under mild conditions, including biologically relevant substrates such as 3,4-dihydroxyphenylalanine (Dopa) and L-adrenaline, with catalytic activity surpassing that of natural enzymes. Nguyen *et al.* functionalized DUT-67 with L-proline (**L41**), preserving MOF crystallinity and enabling precise chiral ligand loading.[129] The resulting DUT-67-pro served as an efficient heterogeneous catalyst for asymmetric Michael additions between cyclohexanone and *trans*-β-nitrostyrene, achieving up to 96% yield with remarkable enantioselectivity. In a follow-up study, the influence of Zr_6-nodes environment on stereoselectivity in aldol reaction of cyclohexanone and 4-nitrobenzaldehyde was explored.[130] Unlike homogeneous L-proline, which typically promotes anti-selectivity,

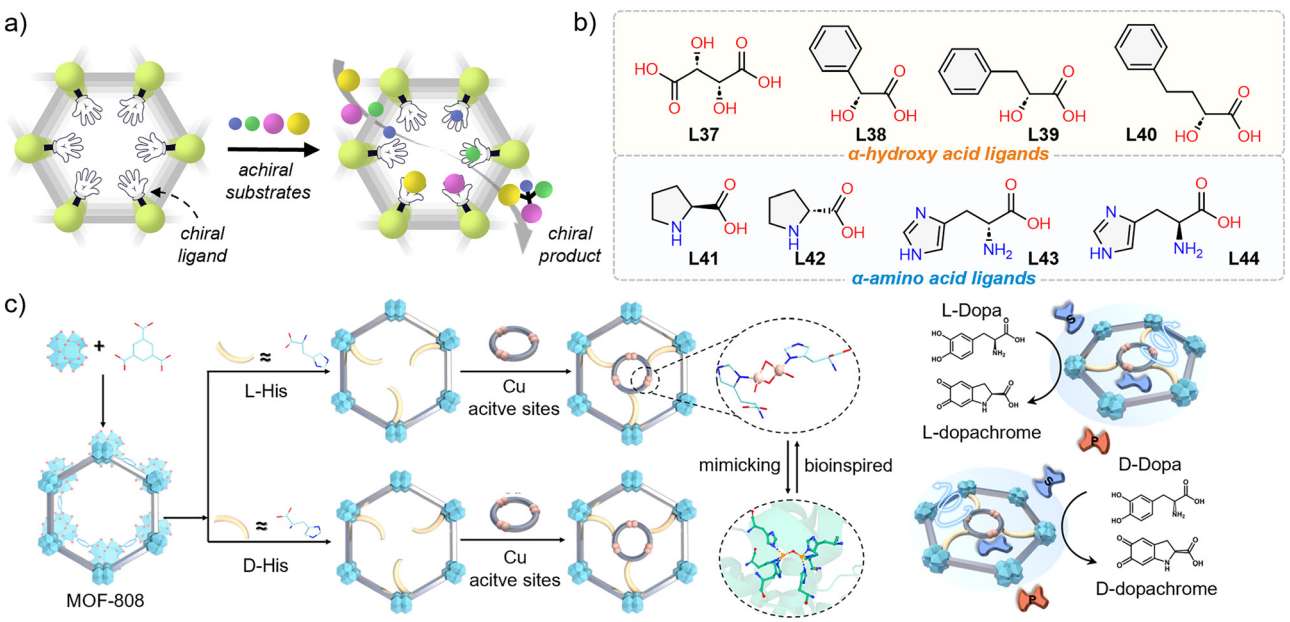

Fig. 6 (a) Scheme of chiral product formation form achiral substrates using CMOF obtained from achiral MOF *via* SALI method. (b) Examples of α-hydroxy and α-amino acid ligands used for SALI. (c) Scheme of two-step functionalization of MOF-808 with L-/D-histidine and Cu(II) ions (left), selective catalytic transformation of L-/D-Dopa to L-/D-dopachrome using L-/D-His-MOF-808 (right).[128] Figure adapted form ref. 128 with permission. Copyright 2023 American Chemical Society.

DUT-67-pro exhibited *syn*-(*S*,*S*) diastereoselectivity. This behavior was attributed to the ability of the Zr_6-nodes to stabilize different transition state geometry at the catalytic site.

4. Other applications of SALI-modified MOFs

In addition to catalytic transformations discussed in the previous chapter, the versatility of the SALI method has enabled its broader applications. This chapter highlights representative examples of SALI-modified MOFs applied to enhance gas adsorption and separation, enable selective sensing platforms, develop drug delivery systems, facilitate energy transfer processes, and construct MOF-polymer hybrids. These examples reflect not only the chemical versatility of SALI method, but also its compatibility with a wide range of structural motifs and application domains. While this chapter focuses on selected studies, the continued evolution of SALI suggests its growing role in multifunctional MOF design across research areas.

4.1. Sorption and separation

The post-synthetic introduction of nonstructural ligands *via* SALI offers a powerful strategy to tune pore environment in MOFs, enhancing their interactions with guest molecules and improving sorption capacities (Fig. 7(a)). Depending on the chemical nature of the introduced ligand, this functionalization can improve affinity towards targeted adsorbates, modulate hydrophilicity/hydrophobicity, or increase overall (hydrolytic) stability. A variety of nonstructural ligands have been installed for these purposes, as summarized in Fig. 7(b).

A well-studied class of ligands used in this context are perfluoroalkane carboxylates, which were introduced into NU-1000 to create SALI-*n* materials, where *n* denotes perfluoroalkyl chain length.[24] These modification enhanced affinity toward CO_2, with SALI-9 showing a notable increase of the heat of adsorption (Q_{st} = 34 kJ mol^{-1}).[24] In a follow-up study, SALI-5 and SALI-9 functionalized with perfluorohexanoic acid and perfluorodecanoic acids (**L45**), respectively, demonstrated improved stability during water adsorption–desorption cycles.[131] The same series of ligands were later applied to NU-1008, where diffusion of BODIPY through the modified pore environments was investigated using combined computational and experimental methods.[132] More recently, Son *et al.* prepared MOF-808 functionalized with a range of phosphonic acid derivatives (**L48–L51**, **L60**) and conducted more comprehensive sorption and permeability studies against series of adsorbates, such as *n*-hexane, propane, benzene and water.[133]

Amino-functionalized compounds (Fig. 7(b)) also represent a major class of ligands for SALI-modified MOFs aimed at selective CO_2 capture, mirroring established industrial amine-based gas treatment systems.[134] For example, incorporation of *N*-α-fluorenylmethyloxycarbonyl (Fmoc)-protected triglycine (**L58**) and 2,6-diacetylaminopyridine-4-carboxylic acid (**L57**) into NU-1000 resulted in enhanced of CO_2 adsorption capacity and selectivity.[135] Similarly, NU-901 functionalized with 3,5-diaminobenzoic acid (**L56**) exhibited over a 130% increase in CO_2 uptake.[136] Post-synthetic grafting of NU-1000 with thiazolium-based ligands (**L59**) created a charged framework with improved CO_2 affinity,[137] while multistep functionalization of MOF-808 with EDTA and ethylenediamine-based linkers introduced multiple amine sites, further enhancing CO_2 adsorption.[138]

Moreover, amino acids due to their zwitterionic nature and diverse functional groups are an intriguing subgroup of ligands that can be used as modulators[139] during MOF synthesis or can be introduced post-synthetically in SALI-like fashion. For example, Lyu *et al.* installed 11 different amino acids into MOF-808 (**L6**, **L41**, **L42**, **L61–L67**), with MOF-808-Lys showing the highest CO_2 uptake improvement as compared to the unmodified MOF-808 (Fig. 7(c)). The investigation of the CO_2 adsorption mechanism in MOF-808-Gly revealed that the uptake of CO_2 under humid conditions leads to the formation of bicarbonates and thus not requiring heat to regenerate the material.[140] In the follow-up study, MOF-808 derivatives functionalized with amino acids were compared to a related system modified with polyamine moieties. In this two-step modification, 3-chloropropionic acid (**L53**) was first installed *via* SALI into MOF-808, followed by nucleophilic substitution with polyamines to generate polyamine-functionalized materials.[141]

Although Zr-MOFs are generally hydrolytically stable across a wide range of pH, the strong capillary forces created during water desorption process can lead to the collapse of porous frameworks. The introduction of nonstructural ligands can reinforce structural integrity and improve water sorption stability in multiple adsorption–desorption cycles. For example, MOF-808 functionalized with EDTA exhibited enhanced resistance to degradation during water sorption (Fig. 7(d)).[142] Similarly, post-synthetic exchange of modulators with other nonstructural ligands in MOF-808[54] and DUT-67[28] can strongly influence sorption properties and stability of the materials. In another example, UiO-67 modified with perfluorooctanoic acid (**L45**) showed improved removal of polycyclic aromatic hydrocarbons (PAHs) from water.[143] Similar approach was employed by Bonnett *et al.* where PCN-222 was modified with myristic acid (**L49**) that improved almost twice water flux in the constructed reverse osmosis membrane while maintaining good salt rejection of $>95\%$.[144]

Beyond carboxylates and phosphonates, other organic molecules have also been explored for enhancing water stability. Liu *et al.* introduced chelating nonstructural ligands based on acetylacetonate and its fluorinated derivatives (**L46**) into NU-1000, observing that the MOF modified with highly hydrophobic fluorinated variant retained structural integrity across 20 water sorption cycles.[145] In contrast, post-synthetic installation of disulfonates such as 1,3-propanedisulfonic acid (**L54**) and 1,5-naphthalenedisulfonic acid (**L55**) in MOF-808 improved hydrophilicity of tested materials and retained their stable water cycling performance.[48] Finally, UiO-66 functionalized with oxalic acid demonstrated improved sorption of several toxic chemicals, including ammonia, cyanogen chloride, SO_2, NO_2, and

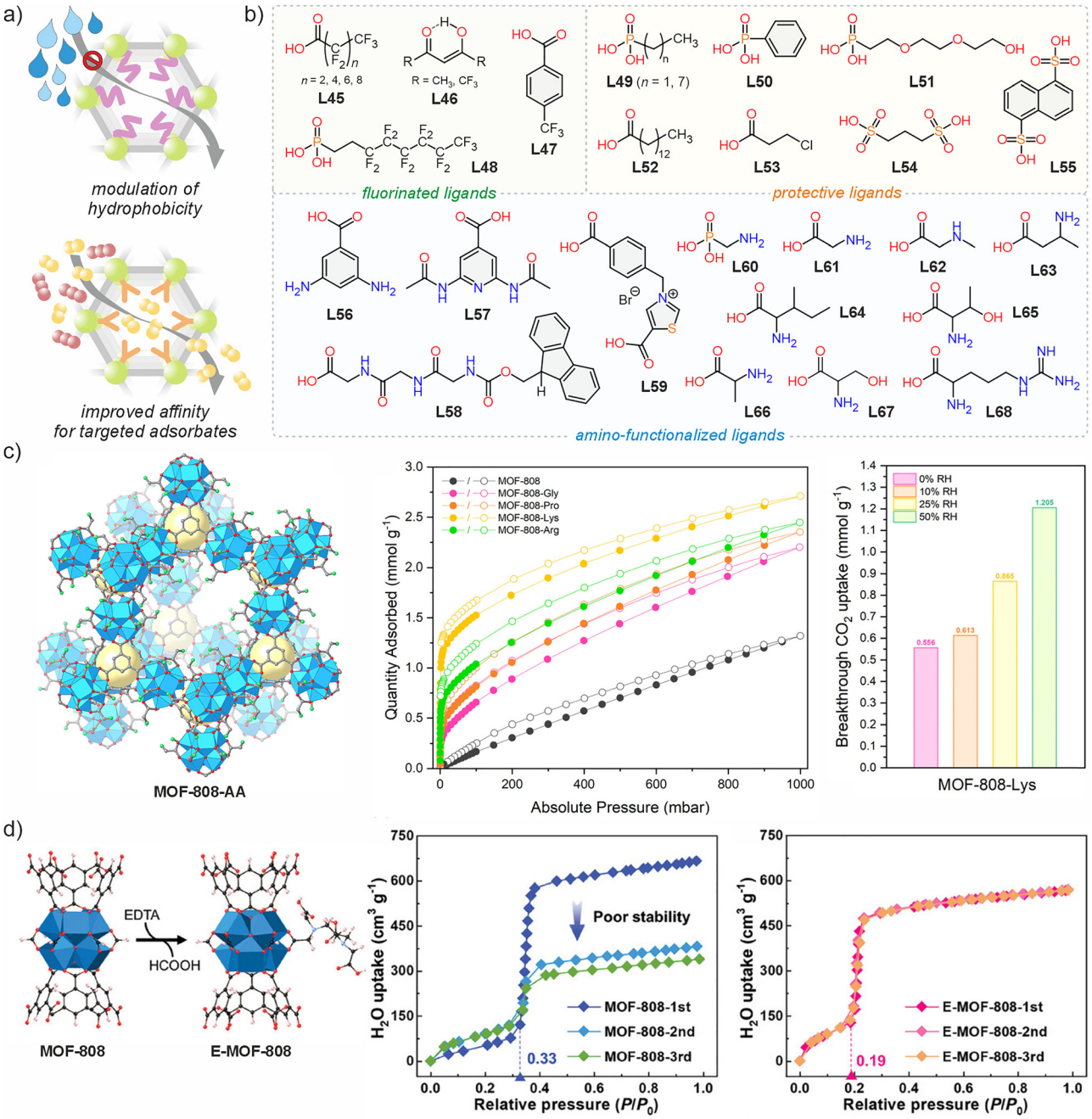

Fig. 7 (a) Schematic representation of SALI-modified MOFs for improved affinity towards targeted adsorbates and enhanced hydrolytic stabilities for water sorption studies. (b) Representative examples of nonstructural ligands incorporated *via* SALI protocol in MOFs for sorption studies. (c) Structure of functionalized MOF-808-AA, where AA = amino acid (left). Comparison of CO_2 sorption isotherms measured at 25 °C for MOF-808 before and after functionalization with series of amino acids (center). Comparison of CO_2 uptakes for MOF-808-Lys by dynamic breakthrough measurements highlighting the water-enhanced uptakes (right).[141] Figure adapted form ref. 140 and 141 with permissions. Copyrights (2022, 2024) American Chemical Society. (d) Schematic representation of 6-connected Zr-nodes of MOF-808 functionalized with EDTA; water sorption isotherms of MOF-808 and functionalized E-MOF-808 measured in three cycles showcasing retained stability of the E-MOF-808 material.[142] Figure adapted form ref. 142 with permission. Copyright 2024 John Wiley and Sons.

octane, highlighting the broader applicability of SALI-based surface modifications for environmental decontamination.[146]

4.2. Chemical sensing

Nonstructural ligands introduced *via* SALI can serve as secondary metal-coordination sites for catalysis (see Section 3.2) but also play a significant role in the design of sensors. This approach was recently demonstrated for MOF-808 which was functionalized with EDTA (**L24**) and subsequently metalated with Cu^{2+} (Fig. 8(c)). The resulting material, MOF-808-EDTA-Cu, acted as an efficient acid vapor sensor capable of visual detection of colorless acid vapors (HCl, HBr, HI). Exposure to

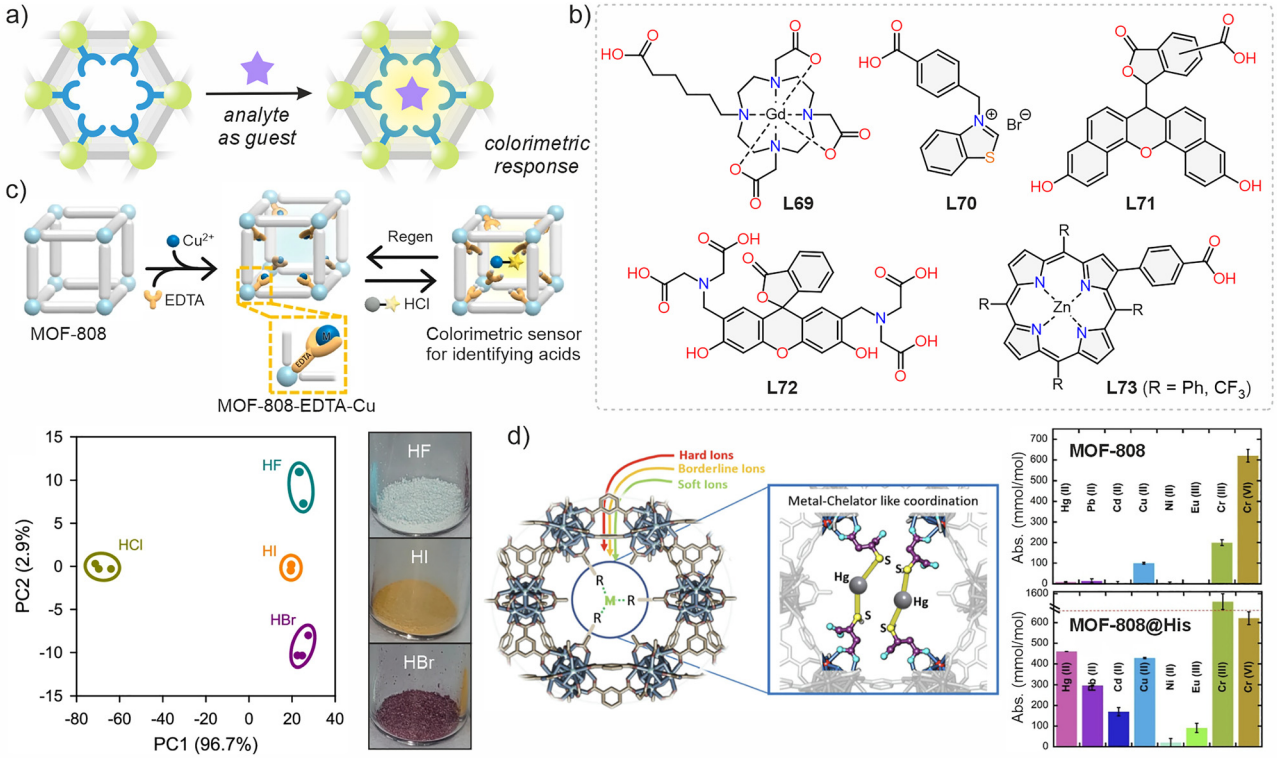

Fig. 8 (a) Scheme of colorimetric detection using SALI-modified MOFs. (b) Representative examples of chromophore molecules introduced *via* SALI for sensing and metal detection studies. (c) Schematic representation of the preparation of MOF-808-EDTA-Cu as an acid vapor decoder (top) and principal component analysis (PCA) results for discrimination of hydrohalic acids showcasing distinctive acid-selective colorimetric behavior with related photographs of MOF-808-EDTA-Cu after exposure to HCl, HBr, and HI vapors (bottom).[62] Figure adapted form ref. 62 with permission. Copyright 2025 Springer Nature. (d) Illustration of hard, borderline, and soft metal–chelator-like traps within the MOF-808 scaffold with possible coordination to Hg(II) in the pore space of functionalized MOF-808. Comparison of adsorption capacity (mmol mol^{-1}) of MOF-808 (top) and MOF-808 functionalized with histidine (bottom) tasted against Hg(II), Pb(II), Cd(II), Cu(II), Ni(II), Eu(III), Cr(III), and Cr(VI).[25] Figure adapted form ref. 25 with permission. Copyright 2022 American Chemical Society.

120 ppm of HCl vapor induced a noticeable color change from cyan to yellow, which was reversible upon immersion in water (~80% regeneration efficiency), thereby ensuring reusability. Furthermore, this sensing platform displayed distinct color changes upon exposure to HF, HBr, and HI, while remaining unaffected by interfering gases, humidity, or temperature (Fig. 8(c)).[62] A similar approach was demonstrated by Pei *et al.*, who prepared a fluorescent sensor based on UiO-67 analogue modified with tartaric acid (**L37**). Subsequent coordination of Tb(III) cations enabled this material to function as a luminescent probe for detection of pesticide nitenpyram.[147] Interestingly, SALI was also utilized to incorporate a Gd(III) complex (**L69**) into NU-1000 and NU-901, which were tested as model magnetic resonance imaging (MRI) contrast agents.[148]

An alternative strategy in sensor design involves introduction of chromophore-based nonstructural ligands to create selective luminescent sensors. For example, NU-1000 functionalized with benzothiazolium bromide (**L70**) was developed as a luminescent sensor for detecting anions (CN^-, SCN^-, OCN^-, $SeCN^-$). This material exhibited a reversible shift in emission from 490 to 450 nm upon anion exposure, accompanied with a color change under UV light.[149] Importantly, the modified material achieved a limit of detection of 1.08×10^{-6} M for cyanide, even in tap water. The post-synthetic installation of pH-sensitive ligand, 5(6)-carboxynaphthofluorescein (**L71**), into NU-1000 led to the construction of a robust colorimetric pH sensor. This material was further tested in detection of byproducts generated during the detoxification of nerve agent simulants.[150] Similarly, pH-dependent fluorescence change was observed in NU-1000 functionalized with 4-aminobenzoic acid (**L16**).[151] Additionally, in biomedical context, coordination of a fluorescent derivative of calcein (**L72**) into selected Zr-MOFs enabled tracking of cellular uptake to study endocytosis pathways.[49,152]

4.3. Heavy metal capture and detection

As demonstrated in Sections 3.2 and 4.2, SALI is a convenient tool for the introduction of ligands bearing functional groups capable of coordinating additional metal centers. This method can be effectively utilized to design functionalized materials tailored for selective heavy metal detection and removal. For example, thiol-bearing carboxylates introduced *via* SALI have been successfully employed for the efficient extraction of heavy metal ions, such as Hg^{2+},[153,154] As^{3+},[155] and Au^{3+}.[156] Additionally, modification of MOF-808 with series of phosphonic acids[53] or amino acids[157] significantly enhanced U(VI) adsorption from aqueous solutions.

Valverde *et al.* carried out a comprehensive study on the post-synthetic modification of Zr-nodes in MOF-808 using a series of eight amino acids, aimed at creating a pore environment rich in diverse functional groups, similar to those found in commercial metal chelators (Fig. 8(d)). The modified MOF materials were screened for adsorption toward different metal cations, followed by multi-component competitive adsorption experiments, where high affinity towards Hg(II), Cd(II) and Pb(II) was observed.[25] In a related approach, MOF- 808 was modified with EDTA (**L24**) to create a multi-ion adsorbent for heavy metals. This material exhibited excellent removal efficiencies (>99%) against 22 heavy metal cations tested in a single-component adsorption, multi-component adsorption, and breakthrough processes.[95]

4.4. Light-harvesting and energy transfer

The introduction of additional chromophores as nonstructural ligands has been explored in the design of artificial light-harvesting systems, enabling MOFs to efficiently absorb light and facilitate energy transfer (EnT) across multiple linkers or molecular units.[158,159] Combining donor and acceptor moieties within MOFs can be achieved through synthesis of multivariate (MTV)-MOFs,[160,161] host–guest integration,[162] and various post-synthetic functionalization strategies, including SALI. Importantly, SALI offers greater precision in ligand positioning compared to mixed-linker approaches, making it more advantageous for ligand-to-ligand EnT mechanistic studies. While a handful of chromophores installed *via* SALI have been discussed for their role in photocatalytic applications (see Section 3.3), the discussion in this section focuses specifically on the fundamental EnT processes.

Due to the ability to precisely control the arrangement of donor and acceptor chromophores, MOFs represent attractive platforms for investigating rapid and long-range energy transfer. One commonly studied pair for EnT includes pyrene (donor) and porphyrin (acceptor), where the emission spectrum of pyrene-based linker overlaps well with the excitation wavelength (420 nm) for porphyrin.[163] The influence of spatial arrangement of these chromophores was explored in 2D Zr-based MOFs composed either of pyrene or porphyrin linkers, where complementary linkers were post-synthetically installed *via* SALI.[164] Two distinct systems were investigated: ''acceptor-on-donor'' (porphyrin linkers immobilized onto pyrene-based MOF) and ''donor-on-acceptor'' (pyrene linkers immobilized onto porphyrin-based MOF). It was found that the ''acceptor-on-donor'' configuration exhibited more efficient energy transfer. Similarly, the SALI functionalization of mesoporous pyrene-based NU-1000 was explored as a model for light-harvesting. Selected monocarboxylate electron acceptors, including porphyrin derivatives[165,166] (**L73**), 3,5-dinitrobenzoate and ferrocene carboxylates,[167,168] were successfully installed *via* SALI, giving a more detailed picture of the influence of spatial arrangement of the chromophores on the EnT processes. It was observed that the two types of accessible pores in the csq topology of NU-1000 enable size-dependent placement of nonstructural ligands, with larger porphyrins preferentially occupying the hexagonal mesopores, while smaller ones (*e.g.* benzoate derivatives) fitting into the triangular micropores.[168]

4.5. Drug delivery

The lability of nonstructural ligands can also be a beneficial property for the controlled release of coordinated guest molecules. This feature can be exploited in drug delivery systems (DDS), where slow or delayed release of bioactive compounds enables targeted therapies with improved efficiency. Typically, MOF-based DDS rely either on weak host–guest interactions, which may result in rapid and uncontrolled cargo release, or on drug molecules covalently attached to organic linkers, where their release requires complete degradation of the MOF. The SALI protocol offers an intermediate solution between these two approaches, enabling greater control over the rate of drug release (Fig. 9(a)).

A wide variety of bioactive molecules have been successfully coordinated to the inorganic nodes of MOFs *via* the SALI approach (Fig. 9(b)). These include nonsteroidal anti-inflammatory drugs such as ibuprofen (**L79**),[45] ketoprofen (**L80**),[169] and diclofenac (**L81**);[170] antibacterial agents including nalidixic acid (**L76**),[169] norfloxacin (**L78**),[171] and levofloxacin (**L77**);[169] and anticancer drugs such as α-cyano-4-hydroxycinnamic acid (α-CHC, **L74**),[152] alendronate (**L75**),[45] and prednisolone,[172] the latter two being phosphate-based drugs. Other biologically relevant ligands, such as folic acid[49] (**L82**, vitamin B_9), biotin[26] (**L83**, vitamin B_7), have also been used for post-synthetic surface functionalization of defective Zr-MOFs.

The direct coordination of the hemilabile drug molecules *via* SALI typically results in moderate release rates, which are strongly influenced by the size of the drug, the available porosity, and the number of free coordination sites in the MOF. As a result, the distribution of the bioactive molecules can vary, ranging from attachment at the external surface of MOF crystallites[26] to more uniform incorporation through the framework, enabling increased overall drug loading.[152,169]

MOFs studied as SALI-based DDS include MIL-100(Fe)[171,172] and several Zr-based materials, such as Zr-fum,[49] UiO-66,[26,45] NU-901,[152,173] and NU-1000.[152,169] Interestingly, the stability of Zr-MOFs is strongly influenced by the composition of the buffer solution used in release studies, particularly due to competitive coordination between phosphate ions and carboxylate ligands.[174] For example, Pander *et al.* reported that the degradation rate of NU-1000 varied significantly depending on the concentration of phosphate-buffered saline (PBS) solution (Fig. 9(c)),[169] and similar trends were also observed for Zr-fum[49] and UiO-66.[175] Consequently, the stability of Zr-MOFs is influenced by both the pK_a of the coordinated linkers and the overall connectivity of the Zr-nodes and linkers.

Abánades Lázaro *et al.* investigated two strategies for introducing drug molecules into microporous UiO-66[26,45] and Zr-fum,[49] where selected bioactive molecules were incorporated either as modulators during synthesis (the coordination modulation approach[26]) or post-synthetically through a SALI-like coordination route. Both drug-loading methods were applied to defective DCA@Zr-MOF materials, in which dichloroacetate

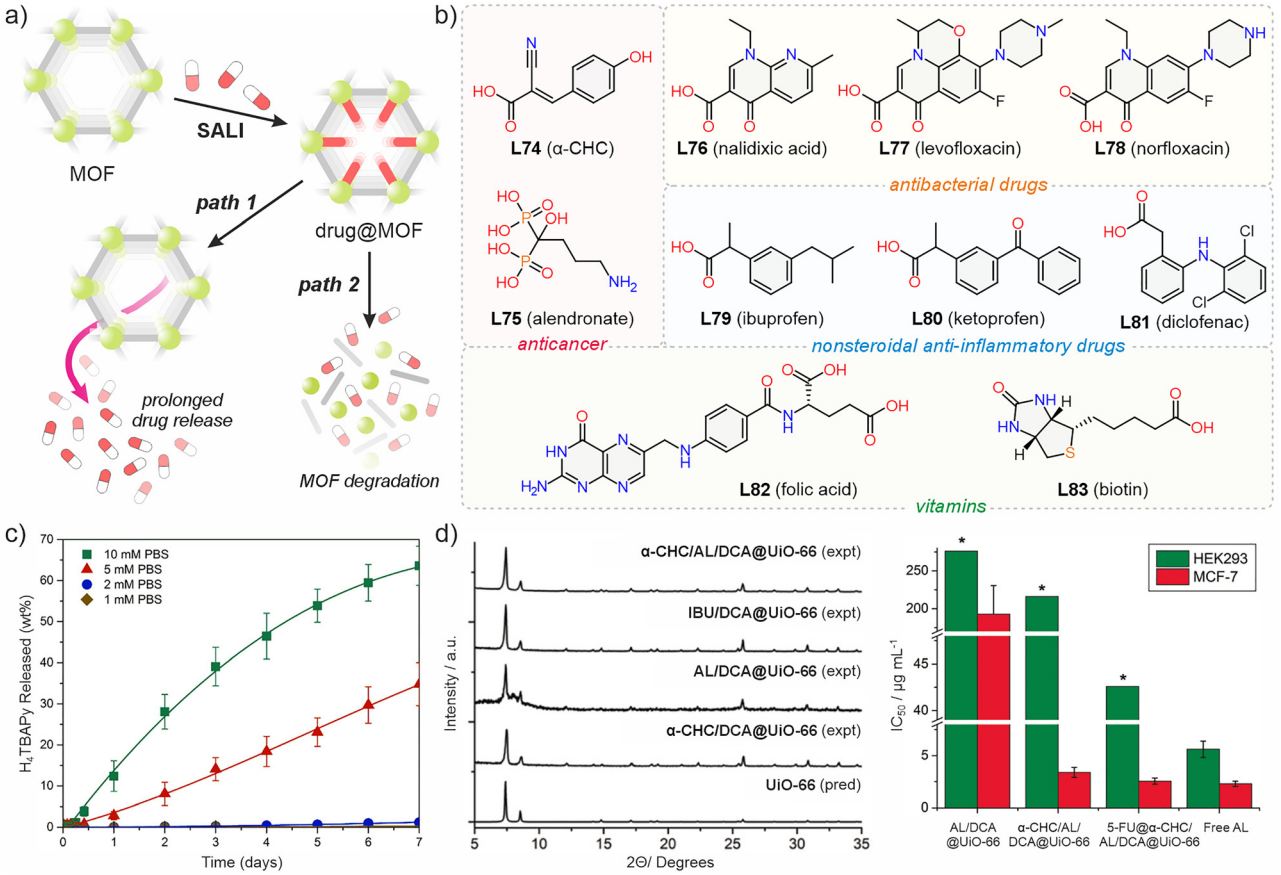

Fig. 9 (a) Scheme of the preparation of SALI-based drug delivery system (drug@MOF) and two possible pathways of drug release: path 1 based on slow discoordination of introduced molecules (reverse-SALI) and path 2 where MOF degradation leads to more rapid drug release.[169] (b) Examples of bioactive molecules introduced into MOF *via* SALI technique; α-CHC = α-cyano-4-hydroxycinnamic acid. (c) Stability in different concentrations of PBS of representative Zr-MOF (NU-1000) studied as drug delivery system.[169] Reprinted from ref. 169 with permission. Copyright 2018 Elsevier. (d) Powder X-ray diffraction (PXRD) patterns of drug-loaded UiO-66 (left) and comparison of IC_{50} values of drug-loaded UiO-66 compared with free alendronate (AL) against HEK293 and MCF-7 cell lines.[45] Figure adapted form ref. 45 with permission. Copyright 2020 John Wiley and Sons.

(DCA) serves as a defect-compensating ligand. The combination of these strategies enabled the preparation of biocompatible UiO-66 material incorporating multiple drug molecules at varying loading levels. One of the key observation was that the inclusion of bisphosphonate-based alendronate (**L75**) enhanced anticancer selectivity, attributed to its strong coordination to Zr-nodes (Fig. 9(d)).[45] These findings were consistent with the work by Christodoulou *et al.*, who compared encapsulation of three prednisolone derivatives in MIL-100(Fe) and reported the highest loading for the phosphate-based analogue, due to its stronger binding affinity to the metal nodes.[172]

4.6. MOF-polymer hybrids

The SALI strategy has also been successfully applied in the preparation of MOF-polymer hybrids. In these systems, polymer chains are directly coordinated to metal nodes of the MOF structure, although this attachment is typically limited to the external surface of MOF crystallites due to the large size and diffusion limitation of polymers. Polymer chains employed in these hybrids possess functional groups capable of binding them directly with the metal nodes.[176] For example, the phospholipid asolectin was post-synthetically coordinated to NU-901, and in combination with the co-polymer F127 formed a unique, functional bilayer with both hydrophobic and hydrophilic regions. This structure significantly improved the protection of the drug-loaded MOF, facilitated its dispersion in aqueous media, and enabled prolonged release of the anticancer drug pemetrexed against two types of cancer cells.[173] Similarly, a series of drug-loaded Zr-MOFs (including PCN-222, UiO-66, MOF-808, NU-901, and PCN-128) were functionalized using methoxy poly(ethylene glycol) phosphate(mPEG-PO_3), where phosphate groups directly coordinated to the Zr-nodes.[177] Such PEGylation strategy notably improved colloidal stability and delayed the release of loaded model drug molecules.

Another intriguing approach for preparation of MOF–polymer hybrids is the reported "click-modulation" method,[26] in which benzoic acid derivatives (**L84**, **L85**) were first introduced as non-structural ligands into UiO-66 (Fig. 10(a)), followed by covalent modification of these functional groups through click reactions with selected polymer chains such as PEG, poly-L-lactide, and poly-*N*-isopropylacrylamide (PNIPAM).[26] The resulting surface-modified UiO-66 crystals exhibited improved stability against

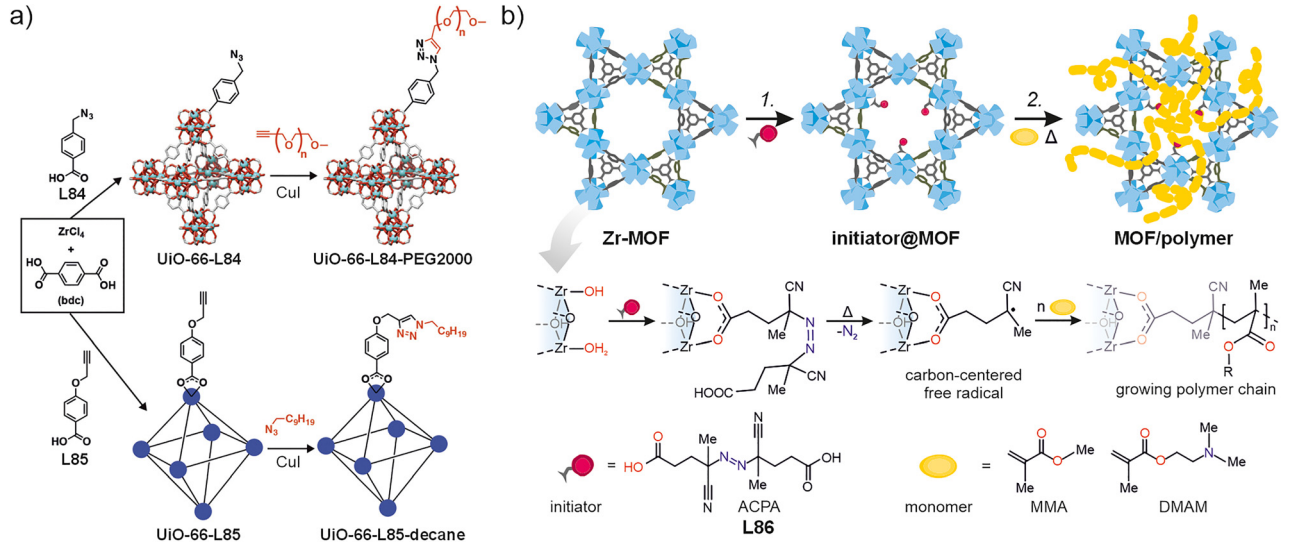

Fig. 10 (a) Scheme of "click modulation" protocol for surface functionalization of UiO-66 using the functionalized ligands **L84** and **L85**. Depending on the introduced functionality, complementary polymers are grafted in secondary step through click reaction.[26] Reproduced from ref. 26 with permission. Copyright 2018 American Chemical Society. (b) Scheme of the two-step protocol for preparation of MOF/polymer hybrids, where ACPA (initiator) is coordinated to Zr-nodes *via* SALI protocol followed by temperature-induced generation of carbon-centered radicals for free-radical polymerization in a MOF (FRaP-in-MOF) of acrylate monomers.[43] Reproduced from ref. 43 with permission from the Royal Society of Chemistry.

phosphate-induced degradation and demonstrated pH-dependent drug release behavior.[50]

Nonstructural ligands have also been employed as anchoring sites for covalent polymer attachment, as demonstrated by the functionalization of UiO-66 with acrylic acid, followed by crosslinking with Arabic gum to form a hybrid hydrogel.[178] The resulting MOF-polymer hybrid showed improved mechanical properties and was evaluated for adsorption of the methylene blue dye.

Recently, a novel strategy for preparation of MOF–polymer hybrids was demonstrated, where Zr-MOFs (NU-1000 and MOF-808) were functionalized with the radical polymerization initiator, 4,4′-azobis(cyanovaleric acid) (ACPA, **L86**).[43] This modification enabled the *in situ* generation of free radicals and polymerization of selected methacrylate monomers with direct attachment of growing polymer chains to the Zr-nodes (Fig. 10(b)). The resulting MOF–polymer hybrids exhibited enhanced mechanical stability and improved catalytic activity toward the hydrolysis of a model nerve-agent simulant.

4.7. Proton and ionic conduction

The SALI strategy can be utilized to tailor proton conduction by introducing nonstructural ligand possessing either proton-donating (–SO_3H, –PO_3H_2, –COOH) and proton-accepting (–OH, –NH_2) groups.[179,180] Several functional nonstructural ligands were successfully coordinated to 6-connected Zr-nodes of MOF-808 which included oxalic acid,[181] EDTA,[181] sulfoacetic acid,[182] 2-sulfoterephthalate,[183] complementary pair of H_2SO_4 and histidine,[184] imidazolium hydrosulfate,[30] imidazolecarboxylates,[185] sulfamates.[186] For example, best performing materials after functionalization of MOF-808 with acidic sulfiliminium moiety achieved proton conduction of 8×10^{-2} S cm^{-1} at 60 °C and 95% relative humidity (RH).[186] Gu *et al.* used 4-sulfobenzoic acid potassium salt (**L20**, Fig. 4) to modify MOF-808 by SALI. The resulting MOF-808-SO_3K-based solid-state electrolyte achieved ionic conductivity of 3.1×10^{-5} S cm^{-1} at 303 K, a low activation energy of 0.32 eV, and a high transference number of 0.76 for potassium ions.[187]

4.8. Beyond SALI: sequential linker installation

The connectivity of the metal nodes can strongly influence the overall stability of a MOF,[188] and introduction of novel nonstructural ligands can, in some cases, contribute to stabilizing of the parent framework.[189] Sequential linker installation (SLI)[190,191] or post-synthetic ligand insertion[192] can be regarded as an extension of SALI method where instead of nonstructural ligands, specially selected linkers can be coordinated to adjacent inorganic nodes (Fig. 11(a)). This approach enables the synthesis of MTV-MOFs with a precise spatial arrangement of linkers[193] and can unlock new topologies that are inaccessible through conventional *de novo* synthetic protocols.[192,194] It has been used to improve the mechanical[195,196] and hydrolytic[197,198] stability, as well as to rigidify otherwise flexible frameworks.[199] For example, the flexible Zr-MOF SIFE-5 was stabilized through post-synthetic coordination of selected linear dicarboxylates between interpenetrated subnetworks, resulting in a rigid analog of the parent structures – SIFE-6 and SIFE-7 (Fig. 11(b)).[200]

Beyond structural stabilization, SLI also provides a versatile tool for introducing new functionalities. In PCN-808, the incorporation of Ru-based dicarboxylates imparted photocatalytic activity,[201] while in PCN-700, the tandem introduction of two additional linkers bearing –COOH and –NH_2 groups enabled bifunctional Brønsted acid–base catalysis.[202] In the NU-606-611 series, careful linker selection allowed tuning hydrophobic

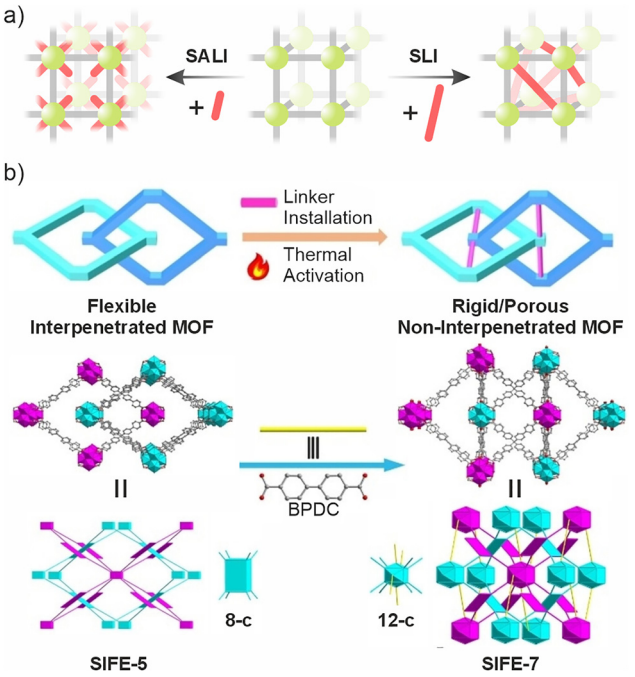

Fig. 11 (a) Scheme of post-synthetic coordination of ligands to inorganic nodes of functionalized MOF showcasing the difference between solvent-assisted ligand incorporation (SALI) and sequential linker installation (SLI). (b) Installation of rigid struts in interpenetrated flexible MOF leads to its rigidification as exemplified in transformation of SIFE-5 to SIFE-7 material.[200] Figure adapted form ref. 200 with permission. Copyright 2025 John Wiley and Sons.

properties, which modulated water sorption behavior.[203] Similarly, in the LIFM-28 system, the choice of secondary linker enabled precise adjustment of catalytic,[204] sorption,[205] and fluorescence[206] properties. A particularly notable case is NPF-320, where a combination of sequential linker installation and exchange led to the incorporation of four different linkers into a single framework, which was used for systematic energy transfer studies.[207]

5. Conclusions and outlook

In this review, we highlighted the role of SALI-modified MOFs in heterogeneous catalysis, with particular attention to their application in acid–base catalysis, photocatalysis, metal immobilization, and asymmetric transformations. Moreover, representative examples of functionalized materials *via* SALI were discussed in sorption and separation processes, sensing, light-harvesting, water treatment, and drug delivery, among others. These cross-disciplinary applications underscore not only the chemical versatility of the SALI approach, but also its compatibility with tandem PSM strategies for increasing complexity of multifunctional systems.

The development of SALI over the last decade has significantly broadened the chemical toolbox for PSM strategies in MOFs by expanding the usefulness of direct coordination of organic ligands to metal nodes. The SALI approach allows precise control over incorporation of functional groups with a minimal disturbance of the integrity of the parent material. As such, a single MOF platform can be tailored for diverse applications by employing carefully designed SALI protocols, as demonstrated throughout this review with numerous examples. Importantly, the SALI protocol can be readily transferable to other MOF systems featuring unsaturated metal nodes and sufficient space to accommodate new ligand coordination types, however, some limitations remain. To date, SALI has been mostly applied to Zr-based MOFs and relies predominantly on carboxylate-based ligands, although other binding motifs, such as phosphonates and sulfonates, have begun to emerge.

Future progress is expected to involve extending SALI to other MOF families featuring accessible coordination sites, expanding the range of usable ligand types, and integrating this method with additional modification strategies. We believe that SALI will remain a compelling and adaptable tool for the rational design of the next-generation MOF-based materials, thanks to its operational simplicity, broad ligand scope and platform compatibility.

Conflicts of interest

There are no conflicts to declare.

Data availability

No primary research results, software nor code have been included, and no new data was generated or analyzed as part of this review.

Acknowledgements

This work was supported by the National Science Centre (NCN) of Poland, grants no. 2024/52/C/ST5/00325 (M. P.) and 2022/47/O/ST4/01081 (M. K.-S., W. B.).

References

1 R. Freund, S. Canossa, S. M. Cohen, W. Yan, H. Deng, V. Guillerm, M. Eddaoudi, D. G. Madden, D. Fairen-Jimenez, H. Lyu, L. K. Macreadie, Z. Ji, Y. Zhang, B. Wang, F. Haase, C. Wöll, O. Zaremba, J. Andreo, S. Wuttke and C. S. Diercks, *Angew. Chem., Int. Ed.*, 2021, **60**, 23946–23974.
2 O. M. Yaghi, M. J. Kalmutzki and C. S. Diercks, *Introduction to Reticular Chemistry: Metal–Organic Frameworks and Covalent Organic Frameworks*, Wiley, Weinheim, 1st edn, 2019.
3 A. Li, R. B. Perez, S. Wiggin, S. C. Ward, P. A. Wood and D. Fairen-Jimenez, *Matter*, 2021, **4**, 1105–1106.
4 R.-B. Lin, S. Xiang, H. Xing, W. Zhou and B. Chen, *Coord. Chem. Rev.*, 2019, **378**, 87–103.
5 A. A. Kotova, D. Thiebaut, J. Vial, A. Tissot and C. Serre, *Coord. Chem. Rev.*, 2022, **455**, 214364.
6 A. Bavykina, N. Kolobov, I. S. Khan, J. A. Bau, A. Ramirez and J. Gascon, *Chem. Rev.*, 2020, **120**, 8468–8535.
7 B. I. Z. Ahmad, K. T. Keasler, E. E. Stacy, S. Meng, T. J. Hicks and P. J. Milner, *Chem. Mater.*, 2023, **35**, 4883–4896.
8 Z. Zhou, M. Vázquez-González and I. Willner, *Chem. Soc. Rev.*, 2021, **50**, 4541–4563.

9 L.-T. Zhang, Y. Zhou and S.-T. Han, *Angew. Chem., Int. Ed.*, 2021, **60**, 15192–15212.
10 M. Kim, M. Pander and H. R. Moon, *ACS Appl. Electron. Mater.*, 2024, **6**, 3024–3038.
11 S. M. Cohen, *Chem. Rev.*, 2012, **112**, 970–1000.
12 Z. Yin, S. Wan, J. Yang, M. Kurmoo and M.-H. Zeng, *Coord. Chem. Rev.*, 2019, **378**, 500–512.
13 M. Kalaj and S. M. Cohen, *ACS Cent. Sci.*, 2020, **6**, 1046–1057.
14 S. Mandal, S. Natarajan, P. Mani and A. Pankajakshan, *Adv. Funct. Mater.*, 2020, **31**, 2006291.
15 P. Deria, J. E. Mondloch, O. Karagiaridi, W. Bury, J. T. Hupp and O. K. Farha, *Chem. Soc. Rev.*, 2014, **43**, 5896–5912.
16 L. Chai, J. Pan, Y. Hu, J. Qian and M. Hong, *Small*, 2021, **17**, 2100607.
17 D. Jędrzejowski, M. Pander, E. Stachura, K. Matlak, W. Bury and D. Matoga, *J. Mater. Chem. A*, 2025, **13**, 23671–23679.
18 C. T. Lollar, J.-S. Qin, J. Pang, S. Yuan, B. Becker and H.-C. Zhou, *Langmuir*, 2018, **34**, 13795–13807.
19 S. Jeoung, S. Kim, M. Kim and H. R. Moon, *Coord. Chem. Rev.*, 2020, **420**, 213377.
20 J. D. Evans, C. J. Sumby and C. J. Doonan, *Chem. Soc. Rev.*, 2014, **43**, 5933–5951.
21 Ü. Kökçam-Demir, A. Goldman, L. Esrafili, M. Gharib, A. Morsali, O. Weingart and C. Janiak, *Chem. Soc. Rev.*, 2020, **49**, 2751–2798.
22 J. Ha, J. H. Lee and H. R. Moon, *Inorg. Chem. Front.*, 2019, **7**, 12–27.
23 S. Abednatanzi, P. G. Derakhshandeh, H. Depauw, F.-X. Coudert, H. Vrielinck, P. V. D. Voort and K. Leus, *Chem. Soc. Rev.*, 2019, **48**, 2535–2565.
24 P. Deria, J. E. Mondloch, E. Tylianakis, P. Ghosh, W. Bury, R. Q. Snurr, J. T. Hupp and O. K. Farha, *J. Am. Chem. Soc.*, 2013, **135**, 16801–16804.
25 A. Valverde, G. I. Tovar, N. A. Rio-López, D. Torres, M. Rosales, S. Wuttke, A. Fidalgo-Marijuan, J. M. Porro, M. Jiménez-Ruiz, V. García Sakai, A. García, J. M. Laza, J. L. Vilas-Vilela, L. Lezama, M. I. Arriortua, G. J. Copello and R. Fernández de Luis, *Chem. Mater.*, 2022, **34**, 9666–9684.
26 I. Abánades Lázaro, S. Haddad, J. M. Rodrigo-Muñoz, C. Orellana-Tavra, V. del Pozo, D. Fairen-Jimenez and R. S. Forgan, *ACS Appl. Mater. Interfaces*, 2018, **10**, 5255–5268.
27 G. Gatto, A. Macchioni, R. Bondi, F. Marmottini and F. Costantino, *Inorganics*, 2019, **7**, 123.
28 F. Drache, V. Bon, I. Senkovska, C. Marschelke, A. Synytska and S. Kaskel, *Inorg. Chem.*, 2016, **55**, 7206–7213.
29 X.-J. Hu, G. Huang, S. Zhang, Z.-B. Fang, T.-F. Liu and R. Cao, *Chem. Commun.*, 2020, **56**, 7459–7462.
30 J. Jia, X.-M. Li, H. Wu, Q. Huang and J. Gao, *ACS Sustain. Chem. Eng.*, 2023, **11**, 13502–13507.
31 Z. Chen, S. L. Hanna, L. R. Redfern, D. Alezi, T. Islamoglu and O. K. Farha, *Coord. Chem. Rev.*, 2019, **386**, 32–49.
32 J. H. Cavka, S. Jakobsen, U. Olsbye, N. Guillou, C. Lamberti, S. Bordiga and K. P. Lillerud, *J. Am. Chem. Soc.*, 2008, **130**, 13850–13851.
33 X. Tang, L. Jia, X. Wang, S. Su, Y. Chen, X.-J. Kong, Z.-M. Ye, H. Xie, W. Gong, E. Du, Y. Liu, K. O. Kirlikovali, O. K. Farha and Y. Cui, *Angew. Chem., Int. Ed.*, 2025, **64**, e202424859.
34 T.-H. Chen, I. Popov and O. Š. Miljanić, *Chem. – Eur. J.*, 2017, **23**, 286–290.
35 Y. Zhang, X. Zhang, J. Lyu, K. Otake, X. Wang, L. R. Redfern, C. D. Malliakas, Z. Li, T. Islamoglu, B. Wang and O. K. Farha, *J. Am. Chem. Soc.*, 2018, **140**, 11179–11183.
36 J. E. Mondloch, W. Bury, D. Fairen-Jimenez, S. Kwon, E. J. DeMarco, M. H. Weston, A. A. Sarjeant, S. T. Nguyen, P. C. Stair, R. Q. Snurr, O. K. Farha and J. T. Hupp, *J. Am. Chem. Soc.*, 2013, **135**, 10294–10297.
37 R. Abazari, S. Sanati, M. A. Bajaber, M. S. Javed, P. C. Junk, A. K. Nanjundan, J. Qian and D. P. Dubal, *Small*, 2024, **20**, e2306353.
38 D. Feng, Z.-Y. Gu, J.-R. Li, H.-L. Jiang, Z. Wei and H.-C. Zhou, *Angew. Chem., Int. Ed.*, 2012, **51**, 10307–10310.
39 H. Furukawa, F. Gándara, Y.-B. Zhang, J. Jiang, W. L. Queen, M. R. Hudson and O. M. Yaghi, *J. Am. Chem. Soc.*, 2014, **136**, 4369–4381.
40 C.-W. Kung, T. C. Wang, J. E. Mondloch, D. Fairen-Jimenez, D. M. Gardner, W. Bury, J. M. Klingsporn, J. C. Barnes, R. Van Duyne, J. F. Stoddart, M. R. Wasielewski, O. K. Farha and J. T. Hupp, *Chem. Mater.*, 2013, **25**, 5012–5017.
41 G. Wißmann, A. Schaate, S. Lilienthal, I. Bremer, A. M. Schneider and P. Behrens, *Microporous Mesoporous Mater.*, 2012, **152**, 64–70.
42 P. Deria, W. Bury, J. T. Hupp and O. K. Farha, *Chem. Commun.*, 2014, **50**, 1965–1968.
43 M. Pander, R. Gil-San-Millan, P. Delgado, C. Perona-Bermejo, U. Kostrzewa, K. Kaczkowski, D. J. Kubicki, J. A. R. Navarro and W. Bury, *Mater. Horiz.*, 2023, **10**, 1301–1308.
44 P. R. McGonigal, P. Deria, I. Hod, P. Z. Moghadam, A.-J. Avestro, N. E. Horwitz, I. C. Gibbs-Hall, A. K. Blackburn, D. Chen, Y. Y. Botros, M. R. Wasielewski, R. Q. Snurr, J. T. Hupp, O. K. Farha and J. F. Stoddart, *Proc. Natl. Acad. Sci. U. S. A.*, 2015, **112**, 11161–11168.
45 I. Abánades Lázaro, C. J. R. Wells and R. S. Forgan, *Angew. Chem., Int. Ed.*, 2020, **59**, 5211–5217.
46 P. Deria, W. Bury, I. Hod, C.-W. Kung, O. Karagiaridi, J. T. Hupp and O. K. Farha, *Inorg. Chem.*, 2015, **54**, 2185–2192.
47 H. Xie, K. O. Kirlikovali, Z. Chen, K. B. Idrees, T. Islamoglu and O. K. Farha, *J. Mater. Chem. A*, 2024, **12**, 6399–6404.
48 T.-Y. Luo, S. Park, T.-H. Chen, Prerna, R. Patel, X. Li, J. Ilja Siepmann, S. Caratzoulas, Z. Xia and M. Tsapatsis, *Angew. Chem., Int. Ed.*, 2022, **61**, e202209034.
49 I. Abánades Lázaro, S. Haddad, J. M. Rodrigo-Muñoz, R. J. Marshall, B. Sastre, V. del Pozo, D. Fairen-Jimenez and R. S. Forgan, *ACS Appl. Mater. Interfaces*, 2018, **10**, 31146–31157.
50 I. Abánades Lázaro, S. Haddad, S. Sacca, C. Orellana-Tavra, D. Fairen-Jimenez and R. S. Forgan, *Chem*, 2017, **2**, 561–578.
51 S. S. Rajasree, J. Yu, S. M. Pratik, X. Li, R. Wang, A. S. Kumbhar, S. Goswami, C. J. Cramer and P. Deria, *J. Am. Chem. Soc.*, 2022, **144**, 1396–1406.
52 K. Hemmer, H. L. B. Boström, S. Krause, B. V. Lotsch and R. A. Fischer, *Commun. Mater.*, 2024, **5**, 1–9.
53 W. Zhang, A. Bu, Q. Ji, L. Min, S. Zhao, Y. Wang and J. Chen, *ACS Appl. Mater. Interfaces*, 2019, **11**, 33931–33940.
54 E. Aunan, C. W. Affolter, U. Olsbye and K. P. Lillerud, *Chem. Mater.*, 2021, **33**, 1471–1476.
55 E. S. Grape, A. M. Davenport and C. K. Brozek, *Dalton Trans.*, 2024, **53**, 1935–1941.
56 R. E. Morris and L. Brammer, *Chem. Soc. Rev.*, 2017, **46**, 5444–5462.
57 L. Jiao, J. Wang and H.-L. Jiang, *Acc. Mater. Res.*, 2021, **2**, 327–339.
58 K. O. Kirlikovali, S. L. Hanna, F. A. Son and O. K. Farha, *ACS Nanosci. Au*, 2023, **3**, 37–45.
59 J. Liu, Z. Li, X. Zhang, K. Otake, L. Zhang, A. W. Peters, M. J. Young, N. M. Bedford, S. P. Letourneau, D. J. Mandia, J. W. Elam, O. K. Farha and J. T. Hupp, *ACS Catal.*, 2019, **9**, 3198–3207.
60 T. M. Rayder, F. Formalik, S. M. Vornholt, H. Frank, S. Lee, M. Alzayer, Z. Chen, D. Sengupta, T. Islamoglu, F. Paesani, K. W. Chapman, R. Q. Snurr and O. K. Farha, *J. Am. Chem. Soc.*, 2023, **145**, 11195–11205.
61 M. Pander, M. Janeta and W. Bury, *ACS Appl. Mater. Interfaces*, 2021, **13**, 8344–8352.
62 W. Jang, H. Yoo, D. Shin, S. Noh and J. Y. Kim, *Nat. Commun.*, 2025, **16**, 385.
63 M. Martos and I. M. Pastor, *ChemistryOpen*, 2025, **14**, e202400428.
64 Y. K. Hwang, D.-Y. Hong, J.-S. Chang, S. H. Jhung, Y.-K. Seo, J. Kim, A. Vimont, M. Daturi, C. Serre and G. Férey, *Angew. Chem., Int. Ed.*, 2008, **47**, 4144–4148.
65 S.-N. Kim, S.-T. Yang, J. Kim, J.-E. Park and W.-S. Ahn, *CrystEngComm*, 2012, **14**, 4142–4147.
66 H. Sepehrmansouri, M. Zarei, M. A. Zolfigol, A. R. Moosavi-Zare, S. Rostamnia and S. Moradi, *Mol. Catal.*, 2020, **481**, 110303.
67 N. Makmeesub, C. Ritvirulh, K. Choojun, S. Sattayaporn, D. E. Resasco and T. Sooknoi, *Catal. Sci. Technol.*, 2022, **12**, 1824–1836.
68 S. Wang, L. Bromberg, H. Schreuder-Gibson and T. A. Hatton, *ACS Appl. Mater. Interfaces*, 2013, **5**, 1269–1278.
69 M. Bahadori, A. Marandi, S. Tangestaninejad, M. Moghadam, V. Mirkhani and I. Mohammadpoor-Baltork, *J. Phys. Chem. C*, 2020, **124**, 8716–8725.
70 Q. Luo, M. Ji, M. Lu, C. Hao, J. Qiu and Y. Li, *J. Mater. Chem. A*, 2013, **1**, 6530–6534.
71 F. Li, Y. Chen, A. Gao, W. Tong, C. Ji, Y. Cheng and Y.-H. Zhou, *New J. Chem.*, 2022, **46**, 18418–18425.
72 J. Long, W. Dai, M. Zou, B. Li, S. Zhang, L. Yang, J. Mao, P. Mao, S. Luo and X. Luo, *Microporous Mesoporous Mater.*, 2021, **318**, 111027.

73 A. Arnanz, M. Pintado-Sierra, A. Corma, M. Iglesias and F. Sánchez, *Adv. Synth. Catal.*, 2012, **354**, 1347–1355.
74 S. Abednatanzi, A. Abbasi and M. Masteri-Farahani, *J. Mol. Catal. Chem.*, 2015, **399**, 10–17.
75 S. Abednatanzi, A. Abbasi and M. Masteri-Farahani, *New J. Chem.*, 2015, **39**, 5322–5328.
76 Q. Luo, X. Song, M. Ji, S.-E. Park, C. Hao and Y. Li, *Appl. Catal., A*, 2014, **478**, 81–90.
77 J. Jiang, F. Gándara, Y.-B. Zhang, K. Na, O. M. Yaghi and W. G. Klemperer, *J. Am. Chem. Soc.*, 2014, **136**, 12844–12847.
78 C. A. Trickett, T. M. Osborn Popp, J. Su, C. Yan, J. Weisberg, A. Huq, P. Urban, J. Jiang, M. J. Kalmutzki, Q. Liu, J. Baek, M. P. Head-Gordon, G. A. Somorjai, J. A. Reimer and O. M. Yaghi, *Nat. Chem.*, 2019, **11**, 170–176.
79 L. H. T. Nguyen, T. T. Nguyen, H. L. Nguyen, T. L. H. Doan and P. H. Tran, *Catal. Sci. Technol.*, 2017, **7**, 4346–4350.
80 V. Roa, S. Cea, C. Pazo, J. Llanos, D. Olivares, N. Escalona, Á. Leiva, Y. Hidalgo-Rosa, X. Zarate, A. Belen Dongil and E. Schott, *Dalton Trans.*, 2025, **54**, 10085–10096.
81 B. Yang, J. I. Wheeler, B. Sorensen, R. Steagall, T. Nielson, J. Yao, J. Mendez-Arroyo and D. H. Ess, *Mater. Adv.*, 2021, **2**, 4246–4254.
82 M. Yabushita, P. Li, T. Islamoglu, H. Kobayashi, A. Fukuoka, O. K. Farha and A. Katz, *Ind. Eng. Chem. Res.*, 2017, **56**, 7141–7148.
83 W. Wang, H. Liu, C. Yang, T. Fan, C. Cui, X. Lu, Z. Tang and G. Li, *Chem. Res. Chin. Univ.*, 2022, **38**, 1301–1307.
84 F. G. Cirujano, N. Martín, G. Fu, C. Jia and D. D. Vos, *Catal. Sci. Technol.*, 2020, **10**, 1796–1802.
85 S. Biswas, R. Gay, J. Bzdrenga, T. Soirot, N. Belverge, N. Taudon, X. Brazzolotto, M. Haouas, N. Steunou, J.-P. Mahy and R. Ricoux, *ChemNanoMat*, 2024, **10**, e202400132.
86 S. J. Garibay, O. K. Farha and J. B. DeCoste, *Chem. Commun.*, 2019, **55**, 7005–7008.
87 S. J. Garibay, T. M. Tovar, I. O. Iordanov, G. W. Peterson and J. B. DeCoste, *J. Mater. Chem. A*, 2023, **11**, 13300–13308.
88 P. Ma, M. Ding, W. Rong, X. Liu and J. Yao, *J. Environ. Chem. Eng.*, 2022, **10**, 108739.
89 M. Chalermnon, S. R. Thomas, J. M. Chin and M. R. Reithofer, *Inorg. Chem. Front.*, 2025, DOI: **10.1039/D5QI01201E**.
90 S. T. Madrahimov, J. R. Gallagher, G. Zhang, Z. Meinhart, S. J. Garibay, M. Delferro, J. T. Miller, O. K. Farha, J. T. Hupp and S. T. Nguyen, *ACS Catal.*, 2015, **5**, 6713–6718.
91 W. Li, C. Zhang, Z. Zheng, X. Zhang, L. Zhang and A. Kuhn, *ACS Appl. Mater. Interfaces*, 2022, **14**, 46673–46681.
92 F. Li, W. E. Housseini, Q. Zhu, L. Zhang, W. Yang and M. Etienne, *Chem. – Eur. J.*, 2024, **30**, e202401893.
93 M. Rimoldi, A. Nakamura, N. A. Vermeulen, J. J. Henkelis, A. K. Blackburn, J. T. Hupp, J. F. Stoddart and O. K. Farha, *Chem. Sci.*, 2016, **7**, 4980–4984.
94 M. S. Alam, X. Li, D. O. Brittin, S. Islam, P. Deria, E. Y. Chekmenev and B. M. Goodson, *Angew. Chem., Int. Ed.*, 2023, **62**, e202213581.
95 Y. Peng, H. Huang, Y. Zhang, C. Kang, S. Chen, L. Song, D. Liu and C. Zhong, *Nat. Commun.*, 2018, **9**, 187.
96 I. Romero-Muñiz, C. Romero-Muñiz, I. del Castillo-Velilla, C. Marini, S. Calero, F. Zamora and A. E. Platero-Prats, *ACS Appl. Mater. Interfaces*, 2022, **14**, 27040–27047.
97 A. Rosado, I.-M. Popa, A. A. Markeb, J. Moral-Vico, E. M. Naughton, H.-G. Eckhardt, J. A. Ayllón, A. M. López-Periago, C. Domingo and L. Negahdar, *J. Mater. Chem. A*, 2024, **12**, 21758–21771.
98 K. Otake, J. Ye, M. Mandal, T. Islamoglu, C. T. Buru, J. T. Hupp, M. Delferro, D. G. Truhlar, C. J. Cramer and O. K. Farha, *ACS Catal.*, 2019, **9**, 5383–5390.
99 S. Goswami, H. Noh, L. R. Redfern, K. Otake, C.-W. Kung, Y. Cui, K. W. Chapman, O. K. Farha and J. T. Hupp, *Chem. Mater.*, 2019, **31**, 1485–1490.
100 S. Muhamed, R. K. Aparna, A. Karmakar, S. Kundu and S. Mandal, *Inorg. Chem.*, 2023, **62**, 7195–7202.
101 S. Muhamed, R. K. Aparna, A. Karmakar, S. Kundu and S. Mandal, *Nanoscale*, 2022, **14**, 17345–17353.
102 Y.-C. Wang, Y.-C. Chen, W.-S. Chuang, J.-H. Li, Y.-S. Wang, C.-H. Chuang, C.-Y. Chen and C.-W. Kung, *ACS Appl. Nano Mater.*, 2020, **3**, 9440–9448.
103 S. Karmakar, S. Barman, F. A. Rahimi, D. Rambabu, S. Nath and T. K. Maji, *Nat. Commun.*, 2023, **14**, 4508.
104 J. Haimerl, G. C. Thaggard, B. K. P. Maldeni Kankanamalage, R. Bühler, J. Lim, K. C. Park, J. Warnan, R. A. Fischer and N. B. Shustova, *J. Am. Chem. Soc.*, 2025, **147**, 19918–19930.
105 A. J. Howarth, C. T. Buru, Y. Liu, A. M. Ploskonka, K. J. Hartlieb, M. McEntee, J. J. Mahle, J. H. Buchanan, E. M. Durke, S. S. Al-Juaid, J. F. Stoddart, J. B. DeCoste, J. T. Hupp and O. K. Farha, *Chem. – Eur. J.*, 2017, **23**, 214–218.
106 W. Jo, H. S. Lee, T. P. Trinh, G. Gupta, M. Kim, G. Y. Kim, J. Kim, C. H. Kim and C. Y. Lee, *ACS Appl. Mater. Interfaces*, 2024, **16**, 69479–69491.
107 H.-G. Jin, W. Lin, H. Sun, P.-C. Zhao, J. Deng and Y. Liu, *Chem. – Eur. J.*, 2025, **31**, e202500015.
108 Q. Xia, J. Yang, S. Zhang, J. Zhang, Z. Li, J. Wang and X. Chen, *J. Am. Chem. Soc.*, 2023, **145**, 6123–6134.
109 A. Atilgan, T. Islamoglu, A. J. Howarth, J. T. Hupp and O. K. Farha, *ACS Appl. Mater. Interfaces*, 2017, **9**, 24555–24560.
110 J. S. Oh, K. C. Park, G. Gupta and C. Y. Lee, *Bull. Korean Chem. Soc.*, 2019, **40**, 128–133.
111 H. Gao, Y. Tang, S. Liu, C. He, H. Li, L. Zhao and C. Duan, *ACS Appl. Mater. Interfaces*, 2024, **16**, 37896–37905.
112 H. Nagatomi, L. C. Gallington, S. Goswami, J. Duan, K. W. Chapman, N. Yanai, N. Kimizuka, O. K. Farha and J. T. Hupp, *ACS Omega*, 2020, **5**, 30299–30305.
113 J. Duan, S. Goswami and J. T. Hupp, *Front. Chem. Eng.*, 2022, **3**, 1–6.
114 C.-W. Kung, S. Goswami, I. Hod, T. C. Wang, J. Duan, O. K. Farha and J. T. Hupp, *Acc. Chem. Res.*, 2020, **53**, 1187–1195.
115 I. Hod, W. Bury, D. M. Gardner, P. Deria, V. Roznyatovskiy, M. R. Wasielewski, O. K. Farha and J. T. Hupp, *J. Phys. Chem. Lett.*, 2015, **6**, 586–591.
116 A. Van Wyk, T. Smith, J. Park and P. Deria, *J. Am. Chem. Soc.*, 2018, **140**, 2756–2760.
117 R. H. Palmer, J. Liu, C.-W. Kung, I. Hod, O. K. Farha and J. T. Hupp, *Langmuir*, 2018, **34**, 4707–4714.
118 L. Xia, W. Zhou, Y. Xu, Z. Xia, X. Wang, Q. Yang, G. Xie, S. Chen and S. Gao, *Chem. Eng. J.*, 2023, **451**, 138747.
119 M. Banerjee, S. Das, M. Yoon, H. J. Choi, M. H. Hyun, S. M. Park, G. Seo and K. Kim, *J. Am. Chem. Soc.*, 2009, **131**, 7524–7525.
120 J. Chen, X. Chen, Z. Zhang, Z. Bao, H. Xing, Q. Yang and Q. Ren, *Mol. Catal.*, 2018, **445**, 163–169.
121 Q. Shili, S. Yangyang, H. Xudong, C. Hongtao, G. Lidi, H. Zhongyu, Z. Dongsheng, L. Xinyao and Z. Sibing, *RSC Adv.*, 2021, **11**, 37584–37594.
122 A. Gheorghe, B. Strudwick, D. M. Dawson, S. E. Ashbrook, S. Woutersen, D. Dubbeldam and S. Tanase, *Chem. – Eur. J.*, 2020, **26**, 13957–13965.
123 X. Feng, H. S. Jena, K. Leus, G. Wang, J. Ouwehand and P. Van Der Voort, *J. Catal.*, 2018, **365**, 36–42.
124 L. Cheng, K. Zhao, Q. Zhang, Y. Li, Q. Zhai, J. Chen and Y. Lou, *Inorg. Chem.*, 2020, **59**, 7991–8001.
125 L. Cheng, Q. Guo, K. Zhao, Y.-M. Li, H. Ren, C.-Y. Ji and W. Li, *Catal. Lett.*, 2023, **153**, 1024–1035.
126 K. Berijani, A. Morsali and J. T. Hupp, *Catal. Sci. Technol.*, 2019, **9**, 3388–3397.
127 G. Yang, W. Shi, Y. Qian, X. Zheng, Z. Meng and H.-L. Jiang, *Angew. Chem., Int. Ed.*, 2023, **135**, e202308089.
128 M. Sha, L. Rao, W. Xu, Y. Qin, R. Su, Y. Wu, Q. Fang, H. Wang, X. Cui, L. Zheng, W. Gu and C. Zhu, *Nano Lett.*, 2023, **23**, 701–709.
129 K. D. Nguyen, C. Kutzscher, F. Drache, I. Senkovska and S. Kaskel, *Inorg. Chem.*, 2018, **57**, 1483–1489.
130 K. D. Nguyen, C. Kutzscher, S. Ehrling, I. Senkovska, V. Bon, M. de Oliveira, T. Gutmann, G. Buntkowsky and S. Kaskel, *J. Catal.*, 2019, **377**, 41–50.
131 P. Deria, Y. G. Chung, R. Q. Snurr, J. T. Hupp and O. K. Farha, *Chem. Sci.*, 2015, **6**, 5172–5176.
132 R. Wang, B. C. Bukowski, J. Duan, K. Zhang, R. Q. Snurr and J. T. Hupp, *ACS Appl. Mater. Interfaces*, 2023, **15**, 51854–51862.
133 F. A. Son, O. J. Bailey, T. Islamoglu and O. K. Farha, *ACS Appl. Mater. Interfaces*, 2024, **16**, 31798–31806.
134 K. Sumida, D. L. Rogow, J. A. Mason, T. M. McDonald, E. D. Bloch, Z. R. Herm, T.-H. Bae and J. R. Long, *Chem. Rev.*, 2012, **112**, 724–781.
135 P. Deria, S. Li, H. Zhang, R. Q. Snurr, J. T. Hupp and O. K. Farha, *Chem. Commun.*, 2015, **51**, 12478–12481.
136 S. J. Garibay, I. Iordanov, T. Islamoglu, J. B. DeCoste and O. K. Farha, *CrystEngComm*, 2018, **20**, 7066–7070.

137 G. Mercuri, M. Moroni, S. Galli, G. Tuci, G. Giambastiani, T. Yan, D. Liu and A. Rossin, *ACS Appl. Mater. Interfaces*, 2021, **13**, 58982–58993.
138 J. M. Park, D. K. Yoo and S. H. Jhung, *Chem. Eng. J.*, 2020, **402**, 126254.
139 O. V. Gutov, S. Molina, E. C. Escudero-Adán and A. Shafir, *Chem. – Eur. J.*, 2016, **22**, 13582–13587.
140 H. Lyu, O. I.-F. Chen, N. Hanikel, M. I. Hossain, R. W. Flaig, X. Pei, A. Amin, M. D. Doherty, R. K. Impastato, T. G. Glover, D. R. Moore and O. M. Yaghi, *J. Am. Chem. Soc.*, 2022, **144**, 2387–2396.
141 O. I.-F. Chen, C.-H. Liu, K. Wang, E. Borrego-Marin, H. Li, A. H. Alawadhi, J. A. R. Navarro and O. M. Yaghi, *J. Am. Chem. Soc.*, 2024, **146**, 2835–2844.
142 M. Cheng, X. Lian, H. Bai, X. Wang, J. Xu, M. Cao and X.-H. Bu, *Adv. Funct. Mater.*, 2025, **35**, 2416241.
143 D. Li, M. Qin, X. Lou, J. Zhu, W. Ma, N. Zhang and M. Lu, *J. Chromatogr. A*, 2024, **1737**, 465463.
144 B. L. Bonnett, E. D. Smith, M. De La Garza, M. Cai, J. V. I. Haag, J. M. Serrano, H. D. Cornell, B. Gibbons, S. M. Martin and A. J. Morris, *ACS Appl. Mater. Interfaces*, 2020, **12**, 15765–15773.
145 J. Liu, R. Anderson, K. M. Schmalbach, T. Sheridan, Z. Wang, N. M. Schweitzer, A. Stein, N. A. Mara, D. Gomez-Gualdron and J. T. Hupp, *J. Mater. Chem. A*, 2022, **10**, 17307–17316.
146 J. B. DeCoste, T. J. Demasky, M. J. Katz, O. K. Farha and J. T. Hupp, *New J. Chem.*, 2015, **39**, 2396–2399.
147 X. Pei, J. Bai, Y. Li and X. Kong, *J. Inorg. Organomet. Polym. Mater.*, 2024, **35**, 2746–2756.
148 S. M. McLeod, L. Robison, G. Parigi, A. Olszewski, R. J. Drout, X. Gong, T. Islamoglu, C. Luchinat, O. K. Farha and T. J. Meade, *ACS Appl. Mater. Interfaces*, 2020, **12**, 41157–41166.
149 L. Luconi, G. Mercuri, T. Islamoglu, A. Fermi, G. Bergamini, G. Giambastiani and A. Rossin, *J. Mater. Chem. C*, 2020, **8**, 7492–7500.
150 S.-Y. Moon, A. J. Howarth, T. Wang, N. A. Vermeulen, J. T. Hupp and O. K. Farha, *Chem. Commun.*, 2016, **52**, 3438–3441.
151 H. Li, Q. Chen, Y. Wang, Z. Zhang, H. Chen, Z. Wang and Z. Gong, *Microchem. J.*, 2023, **187**, 108450.
152 M. H. Teplensky, M. Fantham, P. Li, T. C. Wang, J. P. Mehta, L. J. Young, P. Z. Moghadam, J. T. Hupp, O. K. Farha, C. F. Kaminski and D. Fairen-Jimenez, *J. Am. Chem. Soc.*, 2017, **139**, 7522–7532.
153 J. Kim, J. S. Oh, K. C. Park, G. Gupta and C. Yeon Lee, *Inorg. Chim. Acta*, 2019, **486**, 69–73.
154 X. Li, Z. Jia, H.-W. Tan, Y. Yang and L.-A. Hou, *Sep. Purif. Technol.*, 2025, **354**, 129110.
155 S. A. A. Razavi, Z. Sharifzadeh and A. Morsali, *Inorg. Chem.*, 2024, **63**, 5107–5119.
156 S. Nazri, M. Khajeh, A. R. Oveisi, R. Luque, E. Rodríguez-Castellón and M. Ghaffari-Moghaddam, *Sep. Purif. Technol.*, 2021, **259**, 118197.
157 Z. Ma, C. Sun, D. Lin, W. Yao, H. Hou, D. Wu, X. Guo, X. Yu and X. Wang, *Sep. Purif. Technol.*, 2025, **359**, 130607.
158 J.-L. Wang, C. Wang and W. Lin, *ACS Catal.*, 2012, **2**, 2630–2640.
159 M. C. So, G. P. Wiederrecht, J. E. Mondloch, J. T. Hupp and O. K. Farha, *Chem. Commun.*, 2015, **51**, 3501–3510.
160 K. C. Park, C. Seo, G. Gupta, J. Kim and C. Y. Lee, *ACS Appl. Mater. Interfaces*, 2017, **9**, 38670–38677.
161 S. M. Shaikh, S. Ilic, B. J. Gibbons, X. Yang, E. Jakubikova and A. J. Morris, *J. Phys. Chem. C*, 2021, **125**, 22998–23010.
162 H. Cai, W. Lu, C. Yang, M. Zhang, M. Li, C.-M. Che and D. Li, *Adv. Opt. Mater.*, 2019, **7**, 1801149.
163 M. Kim, J. S. Oh, B. H. Kim, A. Y. Kim, K. C. Park, J. Mun, G. Gupta and C. Y. Lee, *Inorg. Chem.*, 2020, **59**, 12947–12953.
164 P. Cai, M. Xu, S.-S. Meng, Z. Lin, T. Yan, H. F. Drake, P. Zhang, J. Pang, Z.-Y. Gu and H.-C. Zhou, *Angew. Chem., Int. Ed.*, 2021, **60**, 27258–27263.
165 X. Li, J. Yu, D. J. Gosztola, H. C. Fry and P. Deria, *J. Am. Chem. Soc.*, 2019, **141**, 16849–16857.
166 X. Li, J. Yu, Z. Lu, J. Duan, H. C. Fry, D. J. Gosztola, K. Maindan, S. S. Rajasree and P. Deria, *J. Am. Chem. Soc.*, 2021, **143**, 15286–15297.
167 S. Goswami, J. Yu, S. Patwardhan, P. Deria and J. T. Hupp, *ACS Energy Lett.*, 2021, **6**, 848–853.
168 B. Saha, A. Li, S. S. Rajasree, Z. Wang, H. C. Fry, D. Ray and P. Deria, *Small*, 2025, e05900.
169 M. Pander, A. Żelichowska and W. Bury, *Polyhedron*, 2018, **156**, 131–137.
170 K. Jiang, L. Zhang, Q. Hu, X. Zhang, J. Zhang, Y. Cui, Y. Yang, B. Li and G. Qian, *Microporous Mesoporous Mater.*, 2019, **275**, 229–234.
171 P. Yadav, S. Kumari, A. Yadav, P. Bhardwaj, M. Maruthi, A. Chakraborty and P. Kanoo, *ACS Omega*, 2023, **8**, 28367–28375.
172 I. Christodoulou, P. Lyu, C. V. Soares, G. Patriarche, C. Serre, G. Maurin and R. Gref, *Int. J. Mol. Sci.*, 2023, **24**, 3362.
173 X. Liu, J. Obacz, G. Emanuelli, J. E. Chambers, S. Abreu, X. Chen, E. Linnane, J. P. Mehta, A. E. H. Wheatley, S. J. Marciniak and D. Fairen-Jimenez, *Chem. Mater.*, 2024, **36**, 3588–3603.
174 D. Bůžek, S. Adamec, K. Lang and J. Demel, *Inorg. Chem. Front.*, 2021, **8**, 720–734.
175 I. Abánades Lázaro, S. Abánades Lázaro and R. S. Forgan, *Chem. Commun.*, 2018, **54**, 2792–2795.
176 S. Yang, V. V. Karve, A. Justin, I. Kochetygov, J. Espín, M. Asgari, O. Trukhina, D. T. Sun, L. Peng and W. L. Queen, *Coord. Chem. Rev.*, 2021, **427**, 213525.
177 X. Chen, Y. Zhuang, N. Rampal, R. Hewitt, G. Divitini, C. A. O'Keefe, X. Liu, D. J. Whitaker, J. W. Wills, R. Jugdaohsingh, J. J. Powell, H. Yu, C. P. Grey, O. A. Scherman and D. Fairen-Jimenez, *J. Am. Chem. Soc.*, 2021, **143**, 13557–13572.
178 S. C. Ribeiro, H. H. C. de Lima, V. L. Kupfer, C. T. P. da Silva, F. R. Veregue, E. Radovanovic, M. R. Guilherme and A. W. Rinaldi, *J. Mol. Liq.*, 2019, **294**, 111553.
179 L. Zhu, H. Yang, T. Xu, F. Shen and C. Si, *Nano-Micro Lett.*, 2024, **17**, 87.
180 A. Sharma, S. Lee, J. Lim and M. S. Lah, *Bull. Korean Chem. Soc.*, 2024, **45**, 145–156.
181 X. Meng, H.-N. Wang, L.-S. Wang, Y.-H. Zou and Z.-Y. Zhou, *CrystEngComm*, 2019, **21**, 3146–3150.
182 C.-H. Shen, Y.-N. Chang, Y.-L. Chen and C.-W. Kung, *ACS Mater. Lett.*, 2023, **5**, 1938–1943.
183 R. Shi, Z. Zhang, F. Yang and C. Zhong, *Microporous Mesoporous Mater.*, 2022, **343**, 112192.
184 X.-M. Li, J. Jia, D. Liu, M. Xiao and L. Xu, *Inorg. Chem.*, 2025, **64**, 5196–5201.
185 X.-M. Li, Y. Wang, Y. Mu, J. Gao and L. Zeng, *J. Mater. Chem. A*, 2022, **10**, 18592–18597.
186 A. Sharma, J. Lim, S. Jeong, S. Won, J. Seong, S. Lee, Y. S. Kim, S. B. Baek and M. S. Lah, *Angew. Chem., Int. Ed.*, 2021, **60**, 14334–14338.
187 Y.-J. Gu, Y.-A. Lo, A.-C. Li, Y.-C. Chen, J.-H. Li, Y.-S. Wang, H.-K. Tian, W. Kaveevivitchai and C.-W. Kung, *ACS Appl. Energy Mater.*, 2022, **5**, 8573–8580.
188 D. Yang and B. C. Gates, *J. Phys. Chem. C*, 2024, **128**, 8551–8559.
189 V. Bon, N. Kavoosi, I. Senkovska, P. Müller, J. Schaber, D. Wallacher, D. M. Többens, U. Mueller and S. Kaskel, *Dalton Trans.*, 2016, **45**, 4407–4415.
190 Z. Han, Y. Yang, J. Rushlow, R.-R. Liang and H.-C. Zhou, *Acc. Chem. Res.*, 2024, **57**, 3217–3226.
191 M. Bosch, S. Yuan, W. Rutledge and H.-C. Zhou, *Acc. Chem. Res.*, 2017, **50**, 857–865.
192 J. Y. Choi, J. Flood, M. Stodolka, H. T. B. Pham and J. Park, *ACS Nano*, 2022, **16**, 3145–3151.
193 S. Yuan, W. Lu, Y.-P. Chen, Q. Zhang, T.-F. Liu, D. Feng, X. Wang, J. Qin and H.-C. Zhou, *J. Am. Chem. Soc.*, 2015, **137**, 3177–3180.
194 Y. Yang, P. Fernández-Seriñán, B. Ortín-Rubio, P. Samanta, F. Gándara, D. M. Proserpio, D. Nam, J. Juanhuix, I. Imaz and D. Maspoch, *J. Am. Chem. Soc.*, 2024, **147**, 1344–1355.
195 E. A. Kapustin, S. Lee, A. S. Alshammari and O. M. Yaghi, *ACS Cent. Sci.*, 2017, **3**, 662–667.
196 L. Robison, R. J. Drout, L. R. Redfern, F. A. Son, M. C. Wasson, S. Goswami, Z. Chen, A. Olszewski, K. B. Idrees, T. Islamoglu and O. K. Farha, *Chem. Mater.*, 2020, **32**, 3545–3552.
197 Y. Chen, K. B. Idrees, M. R. Mian, F. A. Son, C. Zhang, X. Wang and O. K. Farha, *J. Am. Chem. Soc.*, 2023, **145**, 3055–3063.
198 Z. Lu, H. Tan, H. Lin, X. Cai, L. Du and Q. Liu, *Chem. Mater.*, 2024, **36**, 2652–2660.
199 S.-S. Meng, M. Xu, H. Guan, C. Chen, P. Cai, B. Dong, W.-S. Tan, Y.-H. Gu, W.-Q. Tang, L.-G. Xie, S. Yuan, Y. Han, X. Kong and Z.-Y. Gu, *Nat. Commun.*, 2023, **14**, 5347.
200 H. He, J. Li, J. Zhuang, J. Huang, Y. Meng, X. Lin, Z. Wei, L. Zhang, Y. Fang and M. Pan, *Angew. Chem., Int. Ed.*, 2025, **64**, e202420912.
201 J. Pang, Z. Di, J.-S. Qin, S. Yuan, C. T. Lollar, J. Li, P. Zhang, M. Wu, D. Yuan, M. Hong and H.-C. Zhou, *J. Am. Chem. Soc.*, 2020, **142**, 15020–15026.

202 X.-J. Hu, Z.-X. Li, H. Xue, X. Huang, R. Cao and T.-F. Liu, *CCS Chem.*, 2020, **2**, 616–622.
203 Y. Chen, H. Xie, Y. Zhong, F. Sha, K. O. Kirlikovali, X. Wang, C. Zhang, Z. Li and O. K. Farha, *J. Am. Chem. Soc.*, 2024, **146**, 11202–11210.
204 C.-C. Cao, C.-X. Chen, Z.-W. Wei, Q.-F. Qiu, N.-X. Zhu, Y.-Y. Xiong, J.-J. Jiang, D. Wang and C.-Y. Su, *J. Am. Chem. Soc.*, 2019, **141**, 2589–2593.
205 C.-X. Chen, Z. Wei, J.-J. Jiang, Y.-Z. Fan, S.-P. Zheng, C.-C. Cao, Y.-H. Li, D. Fenske and C.-Y. Su, *Angew. Chem., Int. Ed.*, 2016, **55**, 9932–9936.
206 C.-X. Chen, Q.-F. Qiu, M. Pan, C.-C. Cao, N.-X. Zhu, H.-P. Wang, J.-J. Jiang, Z.-W. Wei and C.-Y. Su, *Chem. Commun.*, 2018, **54**, 13666–13669.
207 Y. Hu, X. Zhang, R. S. H. Khoo, C. Fiankor, X. Zhang and J. Zhang, *J. Am. Chem. Soc.*, 2023, **145**, 13929–13937.

